

THE 1978 TABAS, IRAN, EARTHQUAKE: AN INTERPRETATION OF THE STRONG MOTION RECORDS

BY JAFAR SHOJA-TAHERI* AND JOHN G. ANDERSON

ABSTRACT

The 1978 Tabas, Iran, earthquake ($M_s = 7.4$) was registered on 11 accelerograph stations, with source distances ranging from 3 to 350 km and corresponding recorded peak accelerations ranging from 0.95 down to 0.01 g, respectively. At least four subevents are recognized at Dayhook, the station nearest the epicenter at the southern limit of the fault. The rupture propagated to the northwest with a rupture velocity of 2.7 km/sec. The subevents occurred along the fault as the rupture proceeded.

Curves which describe the distance dependence of peak values of acceleration, velocity, and band-passed acceleration are constructed for this earthquake. Although attenuation of seismic waves is similar in Iran and the Western United States, the prediction curves based on peak strong motion acceleration data from the Western United States systematically underestimate the peak values of the Tabas earthquake and the similar 1952 Kern County earthquake. Prediction curves based on peak velocity in the Western United States overestimate peak velocity for distances less than about 60 km. Site effects are recognized at some recording stations.

The various estimates for stress operating during the earthquake range from 25 to 90 bars. The radiated energy of the main event estimated from accelerograms by two methods is about 2.3×10^{23} ergs, larger than the energy calculated by Gutenberg and Richter energy formula with $M_s = 7.4$. Each of the four subevents released approximately the same amount of energy, corresponding to $M_s \approx 7$. Teleseismic energy estimates for this earthquake are one to two orders of magnitude smaller, indicating large systematic errors exist in one or both of the energy estimation procedures.

INTRODUCTION

On 16 September 1978, a destructive earthquake with an estimated M_s 7.4 (m_b 6.5) occurred in east-central Iran, devastating the town of Tabas with a more than 80 per cent loss of its population, and severely damaging over 90 outlying villages to distances up to 80 km. The total death toll has been estimated to exceed 15,000 (Mohajer-Ashjai and Nowroozi, 1979; Berberian, 1979). The earthquake was strongly felt over an area exceeding 10^6 km², with the highest intensity of shaking (IX-X MM) observed at the town of Tabas and the adjoining villages (see Figure 2 of Berberian, 1979) near the northern limit of the rupture. On the basis of damage and loss of life, this earthquake has been ranked the strongest in this region of Iran during this century (Mohajer-Ashjai and Nowroozi, 1979). As shown in Figure 1, the shock was associated with 75 to 85 km of discontinuous thrust faulting west and northwest of the epicenter (Berberian, 1979; Mohajer-Ashjai and Nowroozi, 1979). Berberian (1979) reported maximum vertical uplift and slip to be about 150 and 300 cm, respectively. The smaller maximum vertical displacement of 0.35 m reported by Mohajer-Ashjai and Nowroozi (1979) is less consistent with teleseismic inferences about the mechanism of the earthquake.

* On sabbatical leave at the Institute of Geophysics and Planetary Physics during the 1985-1986 academic year.

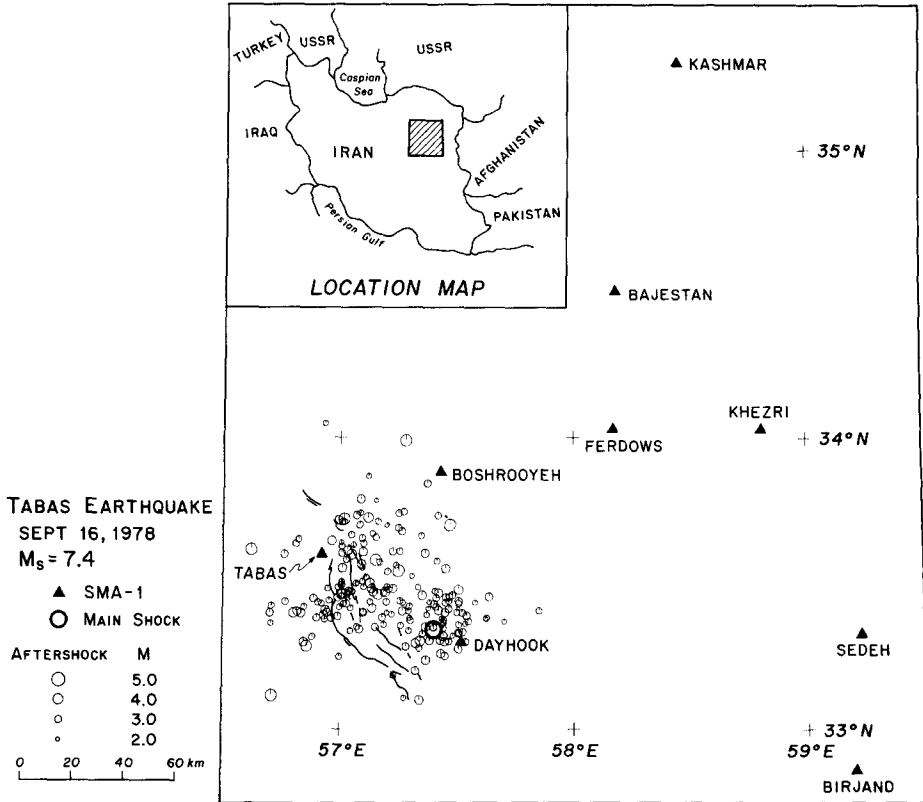


FIG. 1. Map of the region adjacent to the Tabas, Iran earthquake. Faulting (discontinuous lines) is after Berberian (1979), and aftershock locations are after BSNMU (1984). Accelerograms from all stations indicated by solid triangles are studied in this paper.

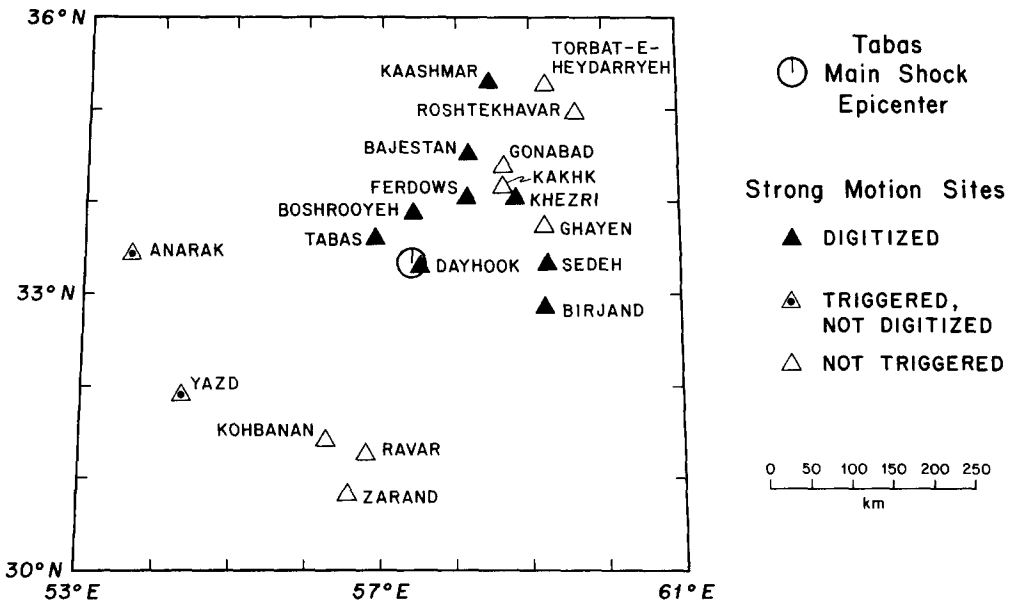


FIG. 2. Network of strong motion stations adjacent to the Tabas epicentral region.

Focal mechanism solutions from teleseismic *P* waves are reported by Berberian (1979) and from surface waves by Niazi and Kanamori (1981). In addition, Berberian (1982) and Niazi and Shoja-Taheri (1985) have given focal mechanism solutions for a number of aftershocks. The various mechanism solutions combined with field observations all indicate a northwest-southeast-trending fault plane dipping toward the east. Information regarding the source parameters of this earthquake reported by various investigators is summarized in Table 1.

During this earthquake, a regional network of 19 strong-motion accelerograph stations equipped with SMA-1 instruments was operating (Figure 2). Among these, 11 stations located within a 3- to 350-km range from the rupture registered the earthquake with peak accelerations of nearly 0.95 to 0.01 g, respectively (see Figures 1 and 2). Recently, Moifar and Adibnazari (1982) published a report containing copies of the accelerograms produced by this earthquake at nine sites within epicentral distances of approximately 250 km. The accelerograms have been digitized, and the report also includes a listing of data at the rate of 50 samples/sec. These data are believed to be the most complete set of accelerograms ever recorded for a shallow intraplate thrust earthquake with magnitude over 7. Therefore, they are very important to both the seismology and engineering communities. Several studies have already been performed on the data in general and, particularly, on the horizontal accelerations recorded at Tabas (Hadley and Mellman, 1982; Hadley *et al.*, 1983; Niazi, 1984; Shoja-Taheri, 1984; Niazi, 1986).

TABLE 1
TABAS EARTHQUAKE SOURCE PARAMETERS OBTAINED FROM PREVIOUS STUDIES

Date:	16 September 1978			
Time:	19 hr, 36 min (local time) 15:35:56.6 GMT (PDE)			
Maximum intensity:	IX to X (Modified Mercalli) (Berberian, 1979)			
Epicenter				
Latitude (°N)	Longitude (°E)	Depth (km)	Magnitude	Source
33.386	57.434	33	7.4 (M_S) 6.5 (m_b)	PDE monthly listing
33.342	57.400	5		BSNMU (1984)
33.35	57.40	5	7.7 (M_L)	Mohajer-Ashjai and Nowroozi (1979)
Moment—Field observations:	1.3 × 10 ²⁷ dyne-cm (Berberian, 1979)			
Normal modes:	1.5 × 10 ²⁷ dyne-cm (Niazi and Kanamori, 1981)			
Long-period <i>P</i> waves:	0.82 × 10 ²⁷ dyne-cm (Niazi and Kanamori, 1981)			
Focal mechanism:	Primarily thrust faulting (Berberian <i>et al.</i> , 1979)			
Fault plane:	Strike 152°, dip 31°E			
Auxiliary plane:	Strike 127°, dip 62°W			
Surface faulting:	Discontinuous and parallel thrust faults, most dip 30° to east (Berberian, 1979)			
Length:	78 km (Berberian, 1982) to 85 km (Berberian, 1979; Berberian <i>et al.</i> , 1979)			
Width:	23 km (Berberian, 1979) based on dip of surface faults and maximum depth of aftershocks 30 km average, 37 km maximum (Berberian <i>et al.</i> , 1979; Berberian, 1982) based on width of aftershock zone			
Slip:	225 cm average, field observations (Berberian, 1979) 300 cm maximum			
Stress drop:	15 to 25 bars (Berberian <i>et al.</i> , 1979; Berberian, 1982) estimate depends on assumed width of faulting			

TABLE 2
ACCELEROGRAPH STATION DATA FROM THE TABAS EARTHQUAKE*

Station	Latitude (°N) Longitude (°E)	Geology ⁽¹⁾	R ⁽²⁾	T _{rec} /T _{dig}	OR ⁽³⁾	A _{max} (cm/sec ²)	V _{max} (cm/sec)	WA ⁽⁴⁾	M _L	A ₀	κ (sec)
Tabas	33.60 56.92	Qf	3	63.5/50.0	N74E(L)	867.0	100.0	4.46	6.5	2.52	0.044
			3		UP(V)	732.0	37.5		2.15	0.011	
			3		N16W(T)	911.0	111.6	4.04	6.5	2.52	0.046
Dayhook	33.30 57.52	K, Nc, or Ev ⁽⁶⁾	18	>51.5/40.0	N80W(L)	366.0	20.6	1.01	6.2	2.01	0.031
			18		UP(V)	185.0	11.7		1.61	0.004	
			18		S10W(T)	393.0	24.7	1.65	6.4	2.06	0.040
Boshrooyeh	33.88 57.43	Qf ⁽⁶⁾	40	>51.0/35.0	N79E(L)	104.0	13.4	0.658	6.7	1.77	0.058
			40		UP(V)	76.0	13.8		1.48	0.024	
			40		N11W(T)	84.0	15.6	0.800	6.8	1.76	0.062
Ferdows ⁽⁷⁾	34.03 58.173	Qf ⁽⁶⁾	115	>51.0/40.0	S20E(L)	97.0	5.5	0.290	7.0	1.66	0.047
			115		UP(V)	52.0	6.9		1.30	0.019	
			115		N70E(T)	104.0	7.2	0.334	7.1	1.63	0.039
Khezri	34.03 58.81	Q or N ⁽⁶⁾	160	20.5/20.5	N61W(L)	25.7	4.4	0.208	7.1	1.08	0.058
			160		UP(V)	23.4	5.5		1.03	0.069	
			160		S29W(T)	24.0	4.6	0.170	7.0	1.07	0.075
Bajestan	34.51 58.18	Qf ⁽¹⁰⁾	161	39.5/39.5	(L)	89.3	7.5	0.215	7.1	1.61	0.056
			161		UP(V)	29.7	4.5		0.953	0.014	
			161		(T)	66.8	4.7	0.137	6.9	1.57	0.059
Sedeh	33.33 59.23	Qf ⁽¹¹⁾	172	>50.7/40.0	N20E(L)	25.5	3.4	0.140	7.0	1.14	0.053
			172		UP(V)	23.5	3.6		0.78	0.032	
			172		N70W(T)	26.8	3.9	0.205	7.2	1.23	0.058
Birjand	32.86 59.20	Qf or Plc ⁽¹²⁾	175	8.5/8.5	N24E(L)						
			175		UP(V)	16.0	3.6				
			175		N66W(T)	18.4	5.1	0.207	7.2		
Kashmar ⁽¹³⁾	35.30 58.45	Qf ⁽¹⁴⁾	250	33.0/33.0	N62W(L)	32.9	9.1	0.329	7.8	1.44	0.089
			250		UP(V)	31.0	9.5		1.03	0.070	
			250		S28W(T)	35.3	9.5	0.361	7.8	1.56	0.094

* Notes:

- All stations are sited on sedimentary deposits. This column gives the mapped geological unit at the site based on the National Iranian Oil Company (1977).

Qf	Quaternary gravel fan or river fan
Qm	Quaternary mud flat
N	Neogene clastics
Nc	Basal Neogene conglomerates
Plc	Pliocene conglomerates
Ev	Eocene intermediate volcanics
K	Cretaceous limestone
Js	Jurassic sandstone and shale.
- Distance is hypocenter distance (depth of 10 km) for all stations but Tabas and Boshrooyeh. Hypocenter distance at these stations is 60 and 73 km, respectively. For these two stations, distance given in the table is distance to the nearest source (fault surface). At Tabas, distance is to the nearest fault outcrop. At Boshrooyeh, distance is to an assumed source at a depth of 10 km and a distance of 17 km east of the surface rupture.
- Component orientations.
- This column shows displacement response of a single degree of freedom oscillator with period 0.8 sec and with damping 0.8. Units are in centimeters. To convert to Wood-Anderson seismometer response (in millimeters), multiply these values by 28,000.
- Station is on alluvium. Town is just inside boundary of mountains, which from map are probably Cretaceous limestone. However secondary roads may take you into Ev within 1-2 km. Coordinates for station are actually 3 km north of town, but we do not know if this is accurate.
- Near boundary of Qp (Quaternary playa) and Qs (sand dunes).
- Ferdows longitude: table in Moinfar and Adibnazari (1982) gives location at 58°, 17 min, not 58.17. Change puts station in town.
- Within errors of coordinates, station may be on Ev (Eocene intermediate volcanics). Just south of Ferdows, geology shows Qb (Quaternary Basalt lava sheets). To west, geology shows, Js (Jurassic sandstone and shale with basal conglomerate).
- Town is not on map. Station coordinates are on boundary of Q and N, both Cenozoic sedimentary formations. Basement is probably Mesozoic limestone, sandstone, or shale.
- Basement to north and northwest is upper Paleozoic to Cretaceous limestone. To east, outcrop of post-Jurassic (Mesozoic, maybe) granite and granodiorite.
- North of Sedeh, outcrop of CM (Cretaceous, maybe) color melange and Cretaceous flysch. To south, Cretaceous and Eocene flyschs. To east, Qb (Quaternary basalt lava sheets). Paleocene conglomerates outcrop to west.
- Ev (Eocene volcanics) outcrop to north. Cretaceous melange outcrops to south.

TABLE 2—Continued

Station	Latitude (°N) Longitude (°E)	Geology ⁽¹⁾	R ⁽²⁾	T _{rec} /T _{dig}	OR ⁽³⁾	A _{max} (cm/sec ²)	V _{max} (cm/sec)	WA ⁽⁴⁾	M _L	A ₀	κ (sec)
Yazd	31.900 54.350	Qf ⁽¹⁵⁾	320	UNK/0.0	(L)						
			320		UP(V)						
			320		(T)						
Anarak	33.433 53.633	Qf ⁽¹⁶⁾	349	UNK/0.0	(L)						
			349		UP(V)						
			349		(T)						
Kakhk	34.158 58.636	Js	156	NT/—	(L)						
			156		UP(V)						
			156		(T)						
Gonabad	34.383 58.650	Qf	174	NT/—	(L)						
			174		UP(V)						
			174		(T)						
Ghayen	33.734 59.192	Qf	177	NT/—	(L)						
			177		UP(V)						
			177		(T)						
Ravar	31.267 56.800	Qf ⁽¹⁷⁾	225	NT/—	(L)						
			225		UP(V)						
			225		(T)						
Kohbanan	31.417 56.267	Qf ⁽¹⁸⁾	227	NT/—	(L)						
			227		UP(V)						
			227		(T)						
Zarand	30.817 56.567	Qf or Qm ⁽¹⁹⁾	279	NT/—	(L)						
			279		UP(V)						
			279		(T)						
Torbat	35.275 59.217	Qf, Ev	283	NT/—	(L)						
			283		UP(V)						
			283		(T)						
Roshtekhabar	34.967 59.633	Qf	283	NT/—	(L)						
			283		UP(V)						
			283		(T)						

13. Kashmar longitude: table gives location at 58°, 45 min, not 58.45. Change puts station in town (in Moinfar and Adibnazari, 1982).

14. Station may be in the mountains north of city. Great Kavir fault runs just north of city and bounds mountains. Station coordinates may be north of this fault (on a Tertiary granite intrusion) or Ev (Eocene Intermediate volcanics).

15. Nearest rock is Triassic, 10 km south of city.

16. Near boundary with Precambrian schists or Quaternary alluvium.

17. Nearest outcrop is Quaternary volcanics.

18. Town is in a valley of Qf. Nearby are extensive outcrops of Js (Jurassic sandstone and shale and related formations) and Plc (Pliocene conglomerates).

19. Nearest mapped outcrop is about 8 km northeast, Paleozoic rocks.

In this study, we analyze the digitized data to illustrate the complexity of the source, and construct attenuation curves for peaks of acceleration, velocity, and band-passed accelerograms. In addition, we estimate some of the source parameters, e.g., rupture velocity, stress drops, and seismic energy release. Two methods to estimate the radiated energy, with possible applications to engineering structural analysis, are introduced and compared.

STRONG MOTION DATA

Table 2 lists all of the regional strong motion stations which were operating at the time of the earthquake. Locations of stations which produced accelerograms in this earthquake, and component orientations are taken from Moinfar and Adibnazari (1982), except as noted. Other locations are coordinates of the nearest town to the station. Geology is based on station location and a geological map of Iran on a scale of 1:1,000,000 (National Iranian Oil Company, 1977). The total duration of

each accelerogram, T_{rec} , was estimated from the figures in Moinfar and Adibnazari (1982), and the duration of the digitized records, T_{dig} , from the digital data. Other columns will be discussed later in this paper.

As reported by Moinfar and Adibnazari (1982), digitization of the recorded accelerograms has been performed by means of SMAC Reader SM-03 at a rate of 50 samples/sec, with no baseline correction. To enhance the quality of the data, after replacing all obvious glitches by linear interpolation from two adjacent points, we employed piecewise baseline correction. This was necessary because of conspicuous deviations of the original digitization from the reproductions of the film records. These deviations had an appearance similar to what would occur if the original film had occasionally slipped on the digitization table during the digitization process. The method we used was to divide the time duration of each record to several segments carefully selected for each individual accelerogram and to apply linear least-squares fit to each segment. Figure 3 compares the uncorrected and baseline-corrected component T of Dayhook to illustrate a typical example of the result of the method. After this processing, we compared the baseline-corrected accelerograms (which we henceforth refer to as the accelerograms) with the copy of the original film to assure that the highest possible fidelity had been achieved. In a few cases, this has caused a significant change in the estimated peak acceleration and its arrival time, since the original digitization deviated quite significantly from the original film copy. We believe our correction has significantly improved the quality of the data.

The corrected accelerograms for all sites are plotted in Figure 4. Integration of accelerograms and high-pass filtering of the velocities were performed in the frequency domain (Shoja-Taheri, 1977). The filter has the amplitude response of that of a Butterworth filter of three poles and corner frequency of 0.125 Hz, but introduced no phase change. Figure 5 shows the velocity time histories of Tabas, Dayhook, Boshrooyeh, and Ferdows. Peak values of acceleration and velocity are listed in Table 2. This table also includes the peak values of the synthetic Wood-Anderson accelerograms, and the estimated local magnitudes, M_L , for each site

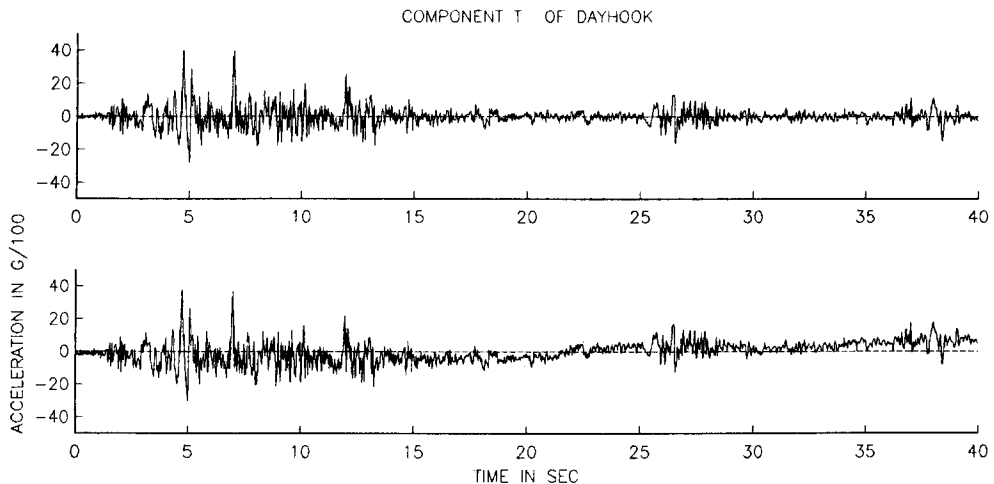


FIG. 3. Acceleration from the transverse (N10E) component at Dayhook as digitized by Moinfar and Adibnazari (1982) (*bottom*), and after subtracting a piecewise-linear function to improve fidelity to a reproduction of the seismogram in the Moinfar and Adibnazari report (*top*).

(Kanamori and Jennings, 1978). The average M_L is 7.0 ± 0.4 .

Several distinct events, within the 40-sec record length of the Dayhook accelerogram, reveal the complexity of the source (Figure 4; Niazi, 1986). The relatively compact arrival of the strong signals on the Tabas records along with other evidence (e.g., location of the epicenter, aftershock distribution, and field observations) strongly suggest propagation of the rupture toward Tabas.

The epicentral coordinates of the event given by both teleseismic and regional observations are all within several kilometers from the Dayhook site (see Table 1 and Figure 1). However, the constrained normal depth (33 km) reported by teleseismic observations (NEIS, Moscow Institute of Physics of the Earth, and ISC) do not agree with the shallow depth (≈ 10 km) given by regional networks (BSNMU and Atomic Energy Organization of Iran) or in addition, the concentration of aftershocks between 8 to 14 km (Berberian, 1982; Niazi and Shoja-Taheri, 1985). Accordingly, a depth of about 10 km seems to be more appropriate for the epicenter of this earthquake.

We have employed the strong motion data to reconsider the epicenter location for the earthquake. As seen from Figures 4 and 5, the epicentral S waves (designated by S_1) can be recognized for each station. Figure 6 shows constraints on the epicenter represented by the arcs drawn for the stations using the corresponding $t_s - t_{trig}$ times.

The $t_s - t_{trig}$ on the Tabas record is apparently too short to have the instrument triggered by the first P arrival. Consequently, there is a high probability of late triggering at Boshrooyeh and Ferdows, also, suggesting that the true epicenter is not likely to be represented by the common point of the arcs of Dayhook, Boshrooyeh, and Ferdows. Assuming that the isolated high-frequency, high-amplitude arrivals of energy at Dayhook labeled S_1, S_2, S_3, S_4 (Figure 4) represent S waves from subevents which occurred sequentially along the fault as rupture proceeds northward (Niazi, 1986), we found plausible locations of the subevents (Figure 6) based on an S -wave velocity of 3.3 km/sec. If the epicenter (circle 1) is farther northeast toward the common point, it is still possible to find corresponding locations for the other subevents, but subevent 4 is moved north of the Tabas station, possibly contradicting the simultaneous arrival of a strong, low-frequency pulse in velocity (identified by R on Figures 4 and 5) which we associate with passage of the rupture at Tabas (Luco and Anderson, 1983, 1985). The polarizations of the initial particle velocity motions at Dayhook and Tabas, also shown in Figure 6, are consistent with the epicenter at circle 1, but calculations with the Haskell (1969) model show that it is equally possible to obtain the same polarizations for an epicenter at other locations on the Dayhook arc within the uncertainty of the rake angle on the fault. We will henceforth refer to circle 1 as the epicenter. Niazi (1986) likewise found that the teleseismic location was not consistent with the local strong motion stations; circle 1 is about 20 km southeast of the epicenter he suggested. The origin time for the subevent at location 4 is about 22 ± 3 sec after the origin time at the epicenter, implying that the rupture velocity is about 2.7 ± 0.2 km/sec. The locations and origin times of subevents 2 and 3 are likewise consistent with propagations of rupture to the north at about this rupture velocity. Subevent 3 is located where the trend of the fault deviates northward, suggesting that the bend of the fault might have been responsible for this burst of energy. Niazi (1984) estimated a rupture velocity of 2.5 km/sec, based on an analysis of the Tabas record alone.

The strongest part of the record from Dayhook, both in velocity and in accelera-

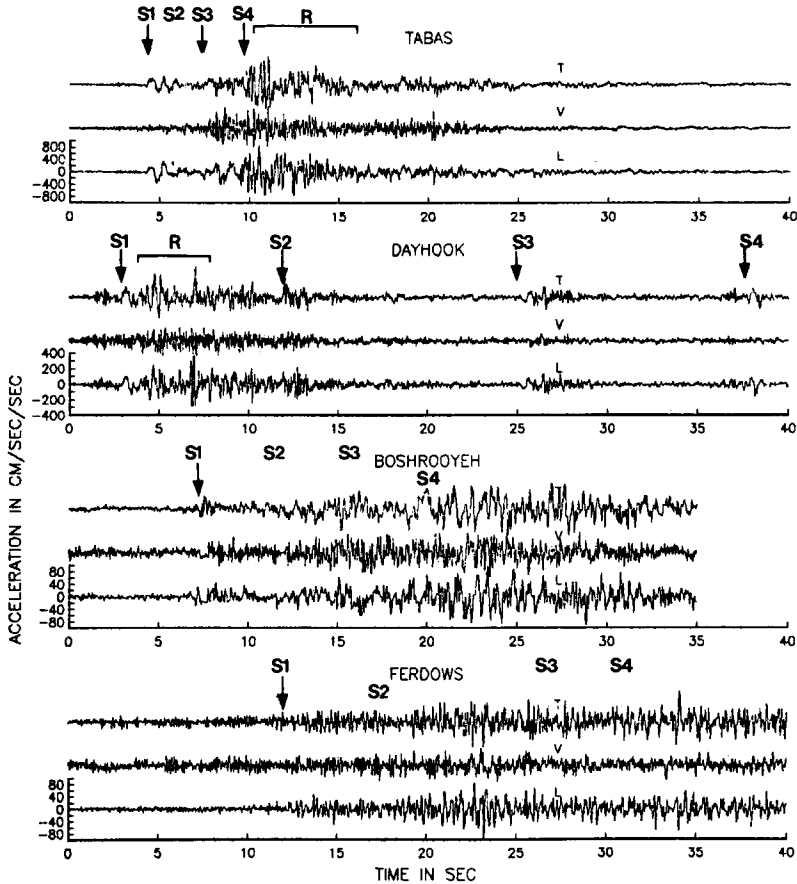


FIG. 4. Digitized portions of all accelerograms from the 1978 Tabas, Iran earthquake. Station locations and component orientations are given in Table 2. Arrows labeled S1, S2, S3, and S4 indicate arrivals which are consistent with subevents 1, 2, 3, and 4 as located on Figure 7. The labels for S2, S3, or S4 which are not associated with arrows indicate approximate arrival times expected from these subevents, but which are not clearly evident. Time windows labeled R indicate approximate time when rupture is nearest the station.

tion, occurs in a time window labeled R, between the pulses labeled S1 and S2. This is apparently associated with details of faulting in the vicinity of the Dayhook site, possibly including some short lengths of rupturing toward the south.

Peak values, attenuation, and Fourier spectra. The accelerograms (Figure 4) depict the extent of shaking at different sites. The town of Tabas, which registered the largest recorded peaks (above 0.9 g) and endured more than 7 sec of shaking which consistently exceeded 0.3 g, suffered the most extensive damage and loss of lives in the region. At Dayhook near the epicenter, the earthquake recorded the second highest peak acceleration of about 0.4 g. Shaking exceeded 0.1 g for nearly 9 sec duration and caused considerable damage to the weak housing units typical of this area. The nearest damage to the Boshrooyeh site was 10 to 15 km to the west (e.g., Mourdestan and Rogheh villages). There was no damage reported in the vicinity of the other accelerograph sites.

Figure 7 shows horizontal peak ground accelerations recorded at nine stations plotted against distance. The peak values from three stations (Kherzi, Birjand, and Kashmar) are lower bounds because the accelerographs triggered late (Figure 4). In

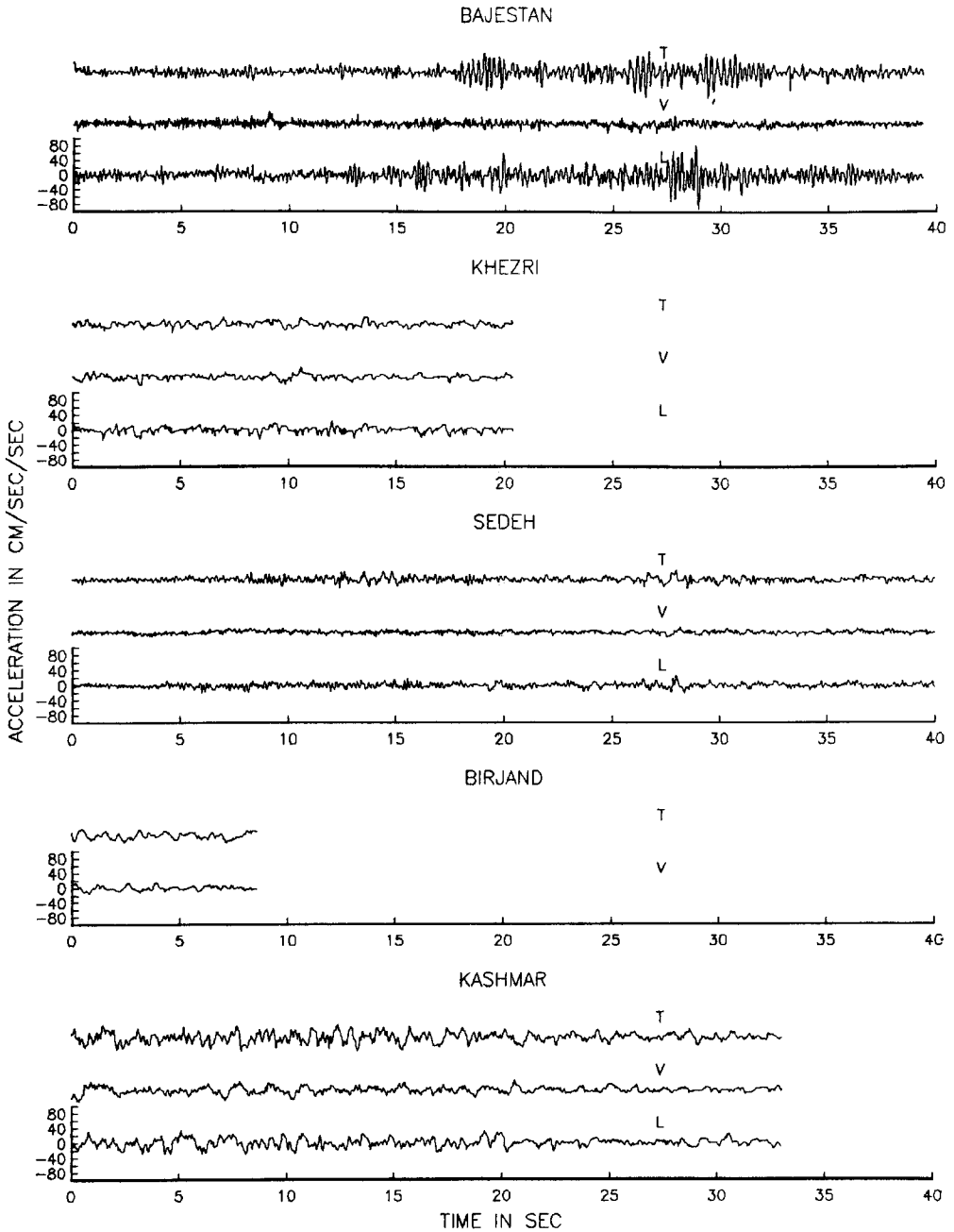


FIG. 4. Continued.

addition, we included the minimum peak values of 10 cm/sec^2 which are usually required (on the vertical component) to trigger the SMA-1 instruments for the sites at Yazd and Anarak (see Table 1 and Figure 2), where small accelerograms were recorded (but not digitized). Between 150 and 250 km, there are five stations which triggered and five which did not. Peak horizontal accelerations at the five stations that did not trigger may have exceeded the nominal vertical-component trigger level. Although Moinfar and Adibnazari (1982) reported that these five stations

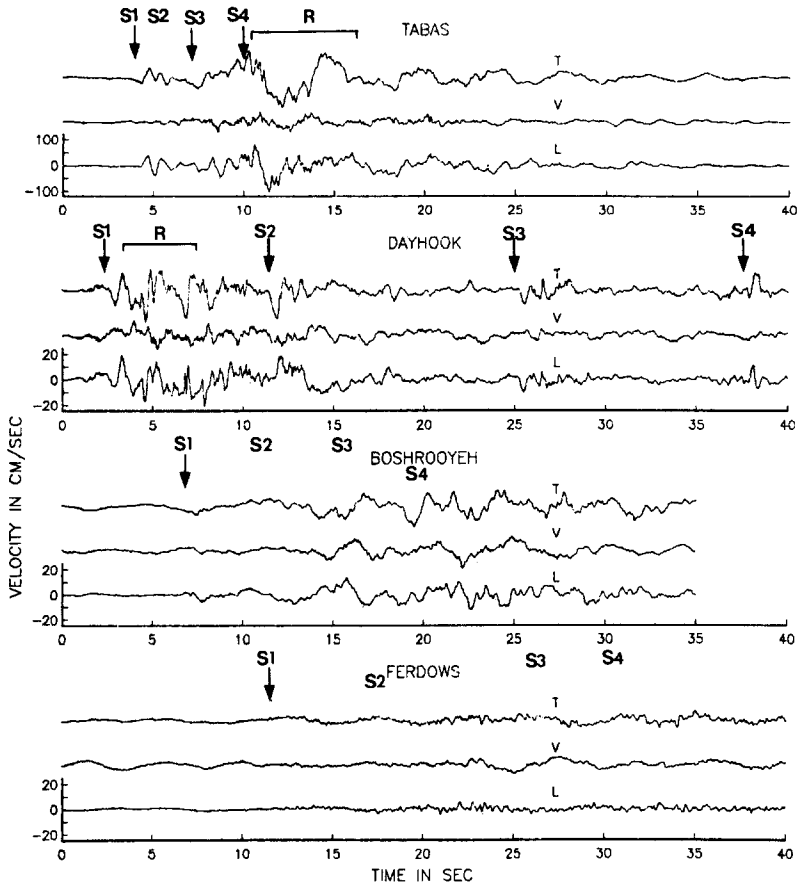


FIG. 5. Velocities of ground motion as inferred from the accelerograms for the four closest stations to the fault rupture. Symbols are the same as in Figure 4.

were all operational, we assume the observations in Figure 7 represent average conditions in this distance range. These peaks are compared with some recently proposed peak ground acceleration prediction curves. As observed by Niazi (1986), most observations from the Tabas earthquake exceed the 50 percentile prediction curves.

Among large intraplate earthquakes ($M_S \geq 7.0$), the three events of Tabas (1978), Kern County, California (1952), and Gazli, USSR (1976) are the known earthquakes which produced close-in strong motion records. The Tabas and Kern County earthquakes are comparable in magnitude and in other parameters (see Tables 1 and 3), and it is therefore of particular interest to compare their corresponding peak ground accelerations in Figure 7. The peak acceleration from the Gazli earthquake has also been included, even though that was a smaller event (Table 3). The result shows that peak values from these earthquakes are consistent with the trend of the Tabas peak values. In Figure 7a, the peak accelerations fall on a trend which lies above the level of the prediction curve of Campbell (1981). Campbell (1981) performed his regression on the average of the two horizontal components, but Tables 2 and 3 show that the average values are very close to the peaks that have been plotted, so that their trend lies above the level of the prediction curve of Campbell. In Figure 7b, there is more scatter in peak values at close distances than

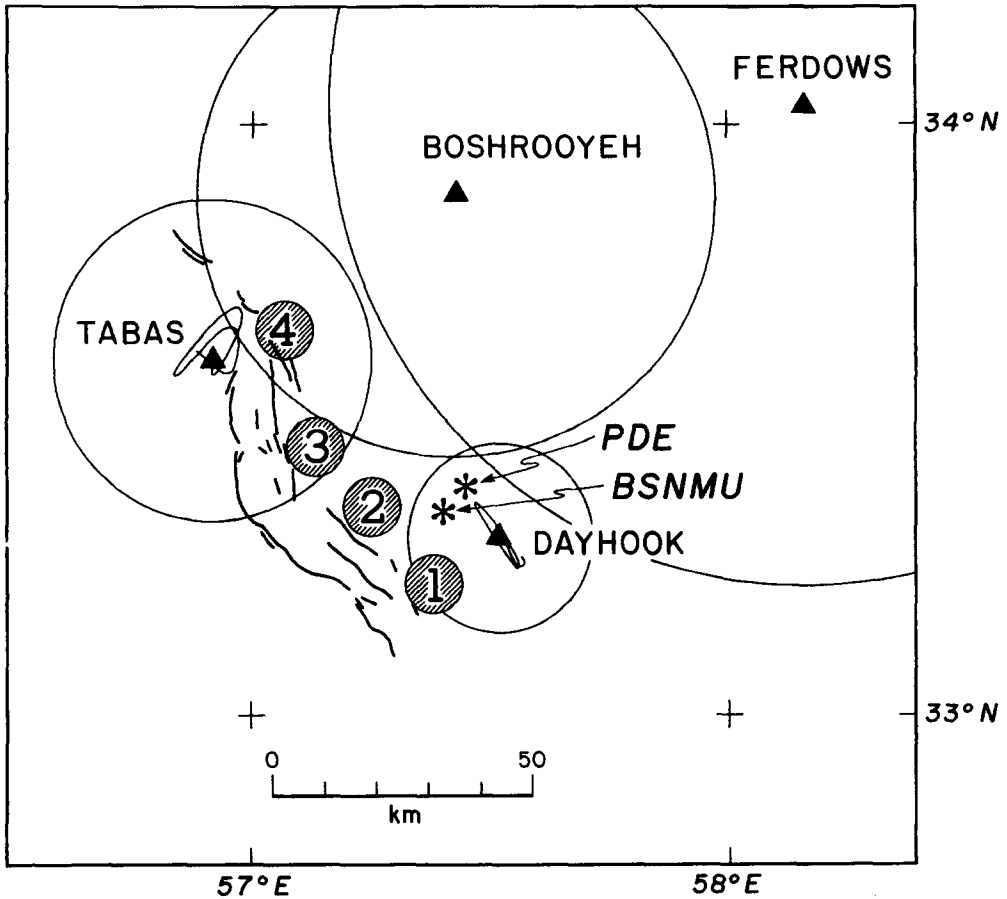


FIG. 6. Map of the epicentral region, showing the four nearest accelerograph locations. Epicenter of the earthquake is constrained to be outside circles centered on each station, which have radii determined from time interval between trigger and first *S* wave. The small shaded circles give a plausible location for four subevents corresponding to the bursts of energy indicated on Figures 4 and 6. The asterisks show location of the epicenter as determined by teleseismic (PDE) and regional (BSNMU) networks. The initial velocity particle motions at Dayhook and Tabas are shown by light lines.

in Figure 7a, due to the different distance assigned to Dayhook. The two prediction curves fall within this scatter at close distances, but at larger distances the peak values are underestimated. Beyond 150 km, the untriggered accelerographs might suggest that the existing points are biased toward high values. We believe that there are too many points in Figure 7 which exceed the prediction curves to be accounted for by unusual local conditions or directivity. Thus, unless all three earthquakes caused above-average shaking due to interearthquake variability (Brillinger and Preisler, 1984), the regressions may systematically underestimate peak accelerations for this type and size of earthquake.

In Figure 8 (a and b), the peak ground velocities calculated at the nine sites are plotted for the same distance measures which were employed in Figure 7 (a and b, respectively). In Figure 8b, they are compared with the 50 percentile peak ground velocity prediction curve introduced by Joyner and Boore (1981, 1982) for $M_w = 7.4$ and for soil sites, and by Joyner *et al.* (1981) for $M_L = 7.0$ and for soil sites. The peak ground velocities calculated for Tabas, Dayhook, and Boshrooyeh are noticeably lower than predicted by the curve. In Figure 8b, the observed peak velocity at

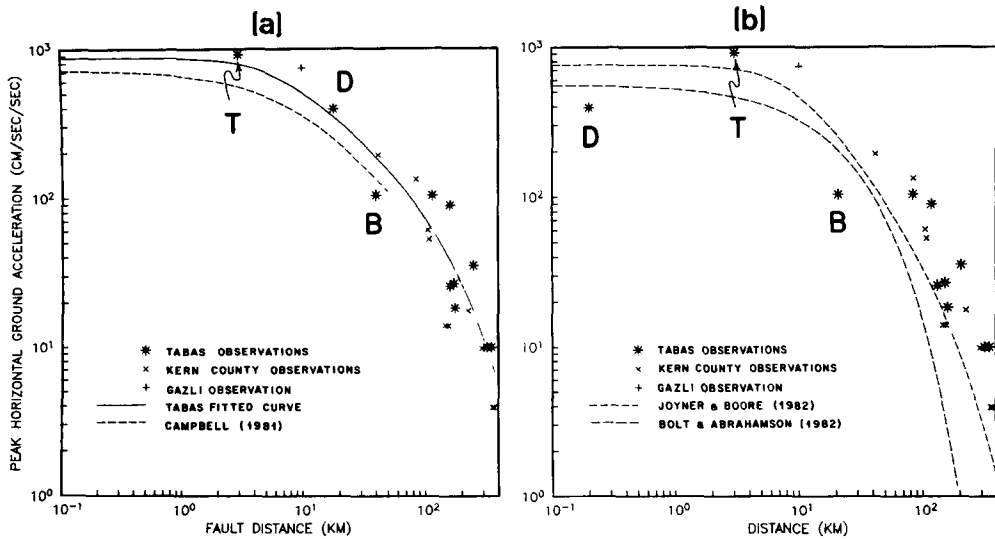


FIG. 7. Distance dependence of peak recorded accelerations (larger of horizontal components) for the Tabas (Table 2), Kern County, and Gazli (Table 3) earthquakes. Distance measure for (a) corresponds to nearest distance to the fault rupture, while distance measure for (b) corresponds to distance to the nearest vertical projection of the rupture. The greatest difference is for the Dayhook site, which is about 15 km from the nearest fault rupture, but directly above it. Points for the Tabas, Dayhook, and Boshrooyeh stations are identified by *T*, *D*, and *B*, respectively. Regressions of Campbell (1981) for $M_S = 7.4$, Bolt and Abrahamson (1982) for $M_w = 7.4$, and Joyner and Boore (1982) for $M_w = 7.4$ are shown on the appropriate plots. Solid line on *left* is a curve which we fit to the Tabas observations.

Dayhook is about an order of magnitude less than predicted; but using the alternative distance measure in Figure 8a, that value falls on a smooth trend consistent with the other observations. The distant sites show higher peak ground velocity values than predicted. Peak ground velocity values of Gazli and Kern County earthquakes follow patterns of attenuation similar to those of the Tabas earthquake. Therefore, it appears that for earthquakes of this size (i.e., $M > 7.0$) the attenuation with distance is less rapid than expected from the Joyner *et al.* regressions.

We also calculated M_L from the strong motion accelerograms (Table 2), following the procedure of Kanamori and Jennings (1978). The average M_L is 7.0 ± 0.4 . The calculated values of M_L depend strongly on the fault distance, increasing by about one M_L unit over the distance range of the sites. The corrections to the Richter (1935, 1958) attenuation curve suggested by Jennings and Kanamori (1983) and by Luco (1982) do not completely remove this distance effect. The distance dependence of M_L is closely related to the failure of the regression curves to predict peak ground velocity correctly, since peak velocity is proportional to peak Wood-Anderson response (Boore, 1980). If one inserts the observed peak velocities into the regression of Joyner *et al.* (1981) and solves for M_L , the resulting values show an increase with distance which mimics the results in Table 2. These discrepancies in Figures 7 and 8 result either from differences in attenuation and structure between Iran and California, or from the effects of extended faulting on near-source stations, which would be general to earthquakes of this size.

Few studies have been made on attenuation of seismic waves in Iran. From isoseismal maps, Chandra *et al.* (1979) concluded that the attenuation of intensities in Iran is slightly more rapid than the San Andreas region attenuation studied by Howell and Schultz (1975). Based on 1-sec period crustal phases of regional

TABLE 3
SOURCE PARAMETERS AND RECORDED PEAK GROUND MOTION PARAMETERS
KERN COUNTY EARTHQUAKE (1952)

Date: 21 July 1952				
Epicenter				
Latitude (°N)	Longitude (°W)	Depth (km)	Magnitude	Source
34.976	119.033	—	7.4-7.7 (M_S) 7.7 (M_S) 7.2 [M_L (sm)]	Dunbar <i>et al.</i> (1980) Kanamori and Jennings (1978) Geller (1976) Kanamori and Jennings (1978)
Moment:		0.90 × 10 ²⁷ dyne-cm (Geller, 1976) 2.0 × 10 ²⁷ dyne-cm (Dunbar, 1980)		
Focal mechanism:		Primarily thrust faulting with left-lateral strike-slip component (Dunbar <i>et al.</i> , 1980)		
Fault plane:		Strike N50E, dip 60°SE (Dunbar <i>et al.</i> , 1980)		
Surface faulting:				
Length:		60 km (Geller, 1976) to 70 km (Dunbar <i>et al.</i> , 1980)		
Width:		18 km (Geller, 1976)		
Left-lateral strike slip:		240 ± 100 cm (Dunbar <i>et al.</i> , 1980)		
Dip slip:		60 to 190 cm (Dunbar <i>et al.</i> , 1980)		
Average slip:		460 cm (Geller, 1976)		
Stress drop:		140 bars (Geller, 1976)		
Strong Motion Data (Murphy and Cloud, 1952; Trifunac and Lee, 1978)				
Station	Distance (km)	Component	PGA (cm/sec/sec)	PGV (cm/sec)
Taft	42	N21E	152.7	15.7
		S69E	175.9	17.7
		Vert	102.8	6.7
Santa Barbara	85	N42E	87.8	11.7
		S48E	128.6	19.3
		Vert	43.6	4.9
Pasadena	109	S00E	46.5	6.2
		S90W	52.1	9.1
		Vert	29.7	3.4
L.A. Hollywood storage	107	S00W	58.1	6.5
		N90E	41.2	8.9
		Vert	20.1	3.2
San Luis Obispo	148	Vert	4	
		234°	10	
		324°	14	
Bishop	224	Vert	6	
		90°	18	
		180°	14	
Colton	156	Vert	12	
		90°	14	
		180°	11	
Hollister	293	Vert	5	
		181°	7	
		271°	10	

TABLE 3—Continued

GAZLI, USSR (1976)				
Date: 19 May 1976				
Epicenter				
Latitude (°N)	Longitude (°E)	Depth (km)	Magnitude	Source
40.35	63.45	14	7.0 M_S , 6.2 m_b 6.35 M_L (sm)	<i>Bulletin of the International Seismological Centre (ISC)</i> Hartzell (1980)
Moment:		1.6 × 10 ²⁶ dyne-cm, Hartzell (1980)		
Focal mechanism:		Primarily thrust faulting, Hartzell (1980)		
Fault plane:		Strike N40E, dip 54°SE, Hartzell (1980)		
Fault area:		150 km ² , Hartzell (1980)		
Average slip:		330 cm, Hartzell (1980)		
Stress drop:		200 bars, Hartzell (1980)		
Strong Motion Data (Hartzell, 1980)				
Station	Distance (km)	Component	PGA (cm/sec/sec)	PGV (cm/sec)
Karakyr Point	20	E-W	738.0	54.0
		N-S	656.0	44.0
		Vert	1300.0	49.0

PGA = peak ground acceleration; PGV = peak ground velocity; Vert = vertical.

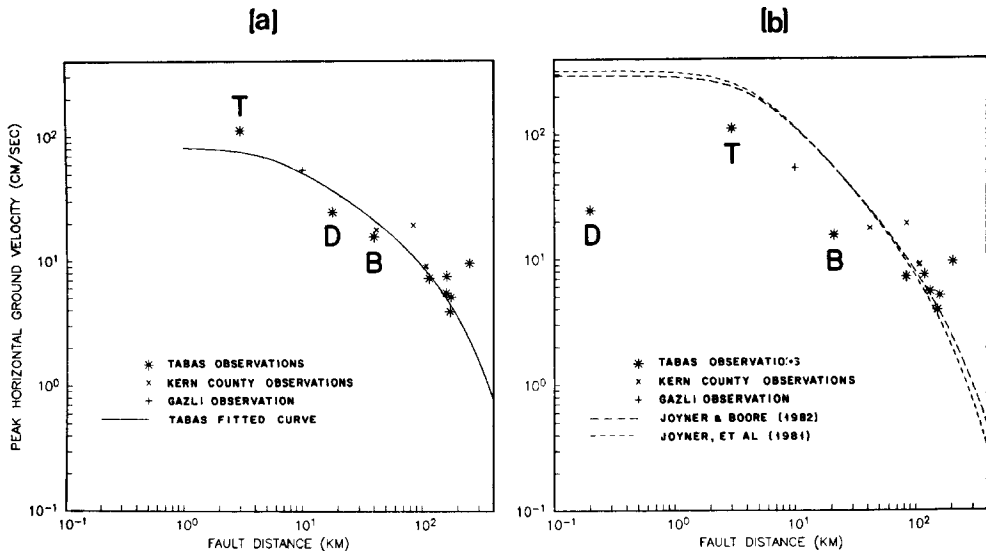


FIG. 8. Distance dependence for peak recorded velocities (larger of horizontal components) for the Tabas (Table 2), Kern County, and Gazli (Table 3) earthquakes. Distance measures are as in Figure 7, a and b. Regressions of Joyner *et al.* (1981) and Joyner and Boore (1982) for $M_w = 7.4$ are shown in (b). Solid line in (a) is a curve which we fit to the observations. The Kashmar station causes the outlier from the curve at left.

earthquakes recorded in Iran, Nuttli (1980) obtained an average value of 0.0045 km⁻¹ for the coefficient of anelastic attenuation, similar to that for California. Both Iran and California have a variety of geological structures and provinces, and therefore one hypothesis is that attenuation in both the Kern County region and the Tabas region differ from the regional average. However, the apparent similarity

of average attenuation in California and Iran makes it more likely that discrepancies between peak values and existing regressions will occur during future earthquakes with magnitudes over about 7.0 in both regions.

We believe that incorporation of the present observations is justified in the next generation of prediction curves and will lead to improvements for estimation of ground motions for large earthquakes. While that is beyond the scope of our study, we have determined attenuation relations from the Tabas earthquake. In fitting these curves, we choose a form similar to that of Joyner and Boore (1981), but with a fixed magnitude

$$\log P = A - B \log R - CR \quad (1)$$

$$R = (d^2 + h^2)^{0.5}.$$

In equation (1), P is the peak value of the ground motion parameter, in our case d is the nearest distance to fault surface, h compensates for energy release occurring away from the nearest point on the fault surface, and A , B , and C are parameters to be determined. Our definition of d differs from the definition by Joyner and Boore (1981), and leads to less scatter about a continuous trend for peak acceleration, peak velocity, and band-pass filtered accelerograms in this instance, and perhaps in general (Campbell, 1981). We found the coefficients to equation (1) in which the parameter P represents the peak ground acceleration, the peak ground velocity, and the peak values of narrow band-passed accelerograms. Because peak accelerations and velocities from Tabas and Kern County follow similar trends, and because the coefficient C is not strongly constrained by the data, we have arbitrarily selected $C = 0.0025$, the value obtained by Joyner and Boore, for all of our relations. Results are listed in Table 4.

The acceleration peaks of the narrow band-passed records are obtained from generalized accelerograms calculated from maximized horizontal spectra at each site (Shoja-Taheri and Bolt, 1977). Within each narrow frequency band, the generalized accelerogram can be visualized as the acceleration on the horizontal

TABLE 4
COEFFICIENTS OF ATTENUATION RELATIONS FOR TABAS DATA

Parameter	Units	A	B	C (km ⁻¹)	h* (km)	σ
Peak acceleration	cm/sec ²	3.40	0.64	0.0025	7.3	0.195
Peak velocity	cm/sec	2.31	0.55	0.0025	4.0	0.123
0.125–1.0 Hz	cm/sec ²	3.02	0.68	0.0025	7.3	0.091
1.0–2.0 Hz	cm/sec ²	3.16	0.66	0.0025	7.3	0.085
2.0–3.0 Hz	cm/sec ²	3.39	0.78	0.0025	7.3	0.188
3.0–4.0 Hz	cm/sec ²	3.23	0.73	0.0025	7.3	0.297
4.0–5.0 Hz	cm/sec ²	3.37	0.82	0.0025	7.3	0.311
5.0–6.0 Hz	cm/sec ²	3.29	0.81	0.0025	7.3	0.311
6.0–7.0 Hz	cm/sec ²	3.27	0.85	0.0025	7.3	0.286
7.0–8.0 Hz	cm/sec ²	3.13	0.84	0.0025	7.3	0.268
8.0–9.0 Hz	cm/sec ²	2.84	0.74	0.0025	7.3	0.229
9.0–10.0 Hz	cm/sec ²	2.89	0.79	0.0025	7.3	0.200
A ₀ (horizontal component)	cm/sec	3.05	0.77	0.000	5.0	0.180
A ₀ (vertical component)	cm/sec	2.69	0.78	0.000	5.0	0.126

* The values for h have been arbitrarily selected identical to those used by Joyner and Boore (1981). For the spectral levels, A_0 , the values for h have been arbitrarily selected as 5 km.

component which is oriented such that it records the maximum ground motion at that frequency. The orientation of the maximum horizontal component varies with frequency. The generalized accelerograms thus eliminate effects due to arbitrary orientation of the horizontal components. The generalized accelerogram at each site is filtered through 10 sequential frequency bands (0.125–1 Hz, 1–2 Hz, ..., 9–10 Hz) using a zero-phase Butterworth filter whose poles increase with frequency. For the Birjand site, band-pass filtering was performed on the only recorded horizontal component. Peak accelerations at different frequency bands are plotted versus source distance in Figure 9. Table 4 lists parameters of the curves which describe the trends in these data.

The coefficients B of $\log R$ range from 0.55 to 0.85 for the correlations listed in Table 4. For body waves from a point source, we expect $B = 1.0$, and for surface waves, we expect $B = 0.5$. The estimated values are within this range, and thus they are reasonable. For a finite source, the fall-off of body-wave amplitudes near the source is less rapid than from a point source (e.g., Schnabel and Seed, 1973; Gusev, 1983), so the values of coefficient B may represent the combined effects of source finiteness at close distances and surface waves at the farther stations. Furthermore, the trend of a more rapid geometrical term shown at higher frequencies is consistent with greater contribution of body waves at high frequencies.

Fourier spectra corresponding to each accelerogram are shown in Figure 10. Fourier spectra of the horizontal components at Tabas reach values well above 100 cm/sec, and the horizontal spectra at Dayhook peak near 100 cm/sec. At the other sites, where there was no damage, spectra are smaller. Except for local variations, they generally show a decrease in the amplitude of shaking with distance. The spectra from Kashmar are larger than those for Bajestan, Khezri, Sedeh, and Birjand. The spectra from Bajestan show a broad, pronounced peak on the horizontal components centered at the frequency of about 4 Hz. The horizontal spectra from the Ferdows station show somewhat smaller amplitudes at longer periods relative to those at the other stations. We believe that these variations are mainly the result of site effects.

We have characterized these spectra by the method of Anderson and Hough (1984). In that paper, the trend of the spectra at high frequencies is described by the function $a(f) = A_0 \times e^{-\pi\kappa f}$, where κ is the spectral decay parameter and A_0 gives the overall level. Table 2 lists the values of A_0 and κ determined from the whole-record spectra, over the frequency band of 1 to 15 Hz. As in Anderson and Hough, we found that the spectra are generally fit satisfactorily by the exponential decay model. The most severe exception was the horizontal components at Bajestan, which show a strong peak at about 4 Hz.

Figure 11 shows a plot of the values of A_0 and κ , as a function of distance, separated by vertical and horizontal components. We first consider the values of κ for the horizontal components, which may be compared with the κ 's for S waves found by Anderson and Hough (1984). Our values are about 0.04 sec for the nearest stations and increase gradually with distance at a rate comparable to that found in California. This increase in κ with distance can only be an effect of attenuation (Anderson and Hough, 1984; Anderson, 1986), and the similar rate again confirms that the attenuation in Iran appears to be about the same as in California. We find that the κ from the vertical components of these records are considerably smaller than the κ 's for the horizontal components. This result is different from the result of Hough *et al.* (1988) and Hough and Anderson (1988), where κ 's from vertical P waves and horizontal S waves observed at Anza, California, are about the same.

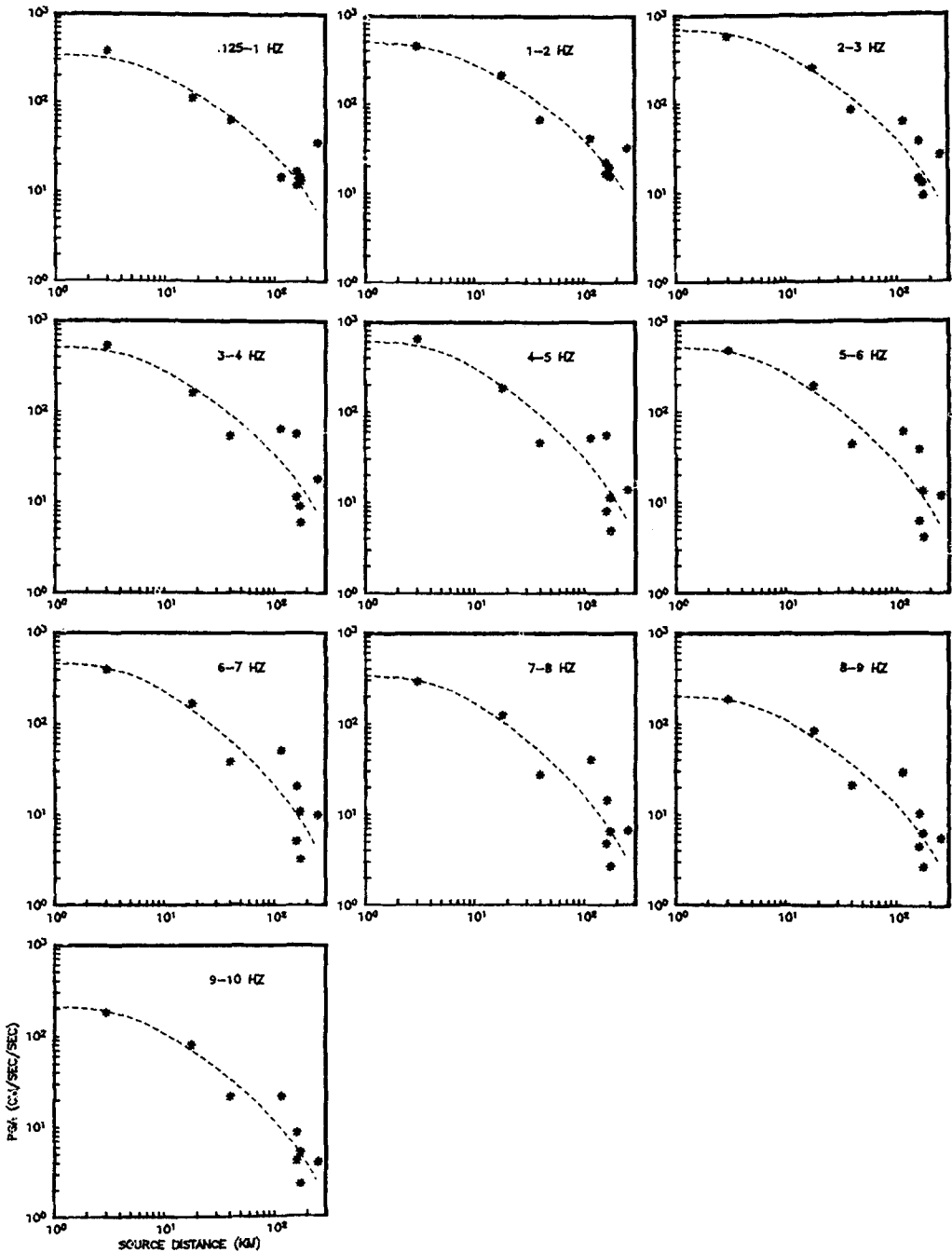


FIG. 9. Peak values of narrow band-passed accelerograms as a function of distance. Orientation of the horizontal components has been rotated to maximize the peak value, following the method of Shoja-Taheri and Bolt (1977).

Figure 11 also shows the values of A_0 plotted as a function of distance for the horizontal and vertical spectra. These values are compared with attenuation curves proportional to $r^{-0.5}$ and $r^{-1.0}$. Consistent with these regression results, the falloff is between these two values. Table 4 gives parameters for a fit of A_0 as a function of

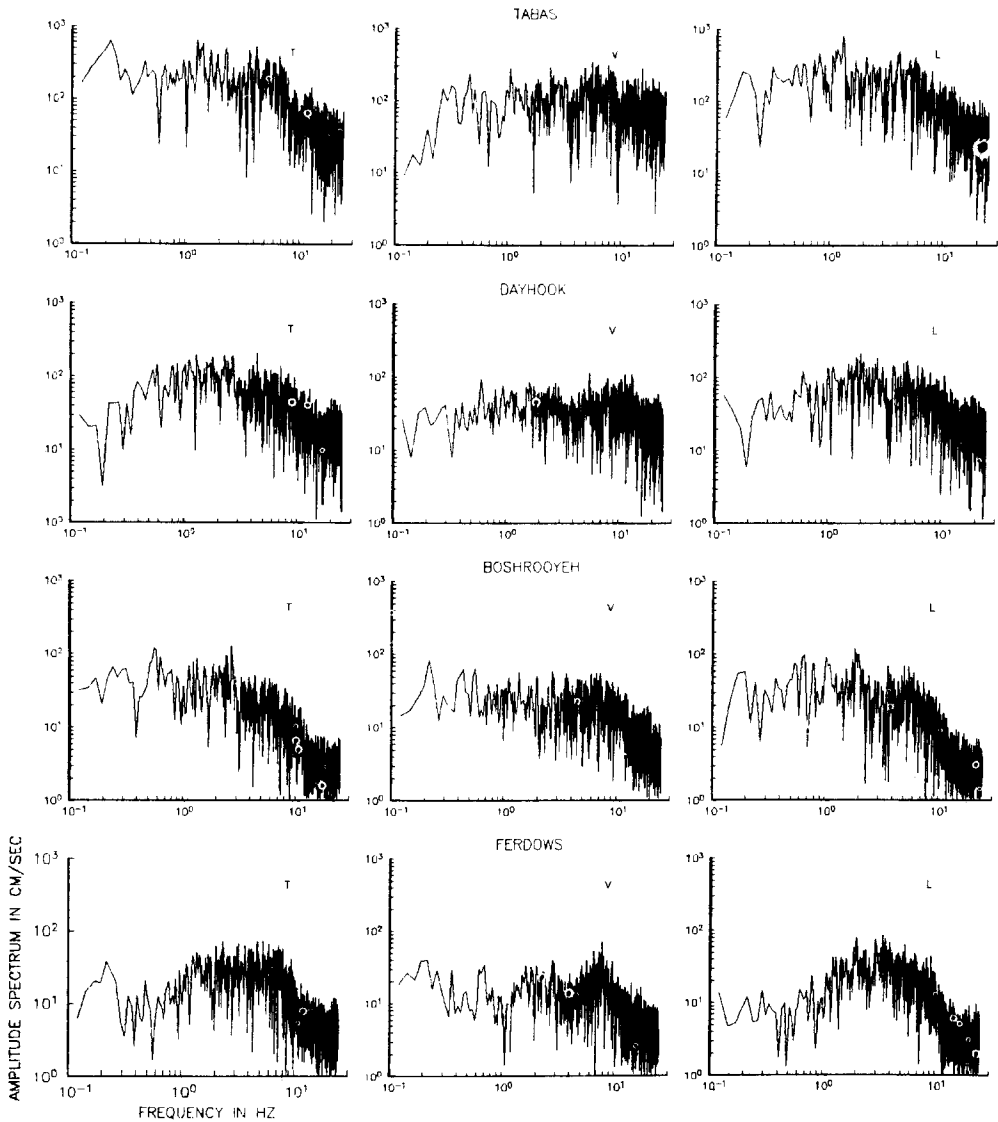


FIG. 10. Fourier amplitude spectra corresponding to all accelerograms in Figure 4.

distance. For small southern California earthquakes, Hough *et al.* (1988) find that A_0 decreased more rapidly than r^{-1} , indicating a frequency-dependent contribution to the total Q . The large fault size in the case of the Tabas event might be responsible for the weaker dependence in distance.

Seismic energy. It is important to calculate the radiated energy. An emerging issue is to reconcile energy estimates obtained from accelerograms with estimates obtained from teleseisms. From the Tabas records, we can provide a near-field test of the relationship proposed by Gutenberg and Richter (1954) based on the teleseismic data and estimate the apparent stress drop of the earthquake. In addition, the energy density represented by an individual seismogram has engineering applications for nonlinear analysis, so we are interested in improving the methods to relate this to the total radiated energy, with eventual applications to seismic hazard estimation.

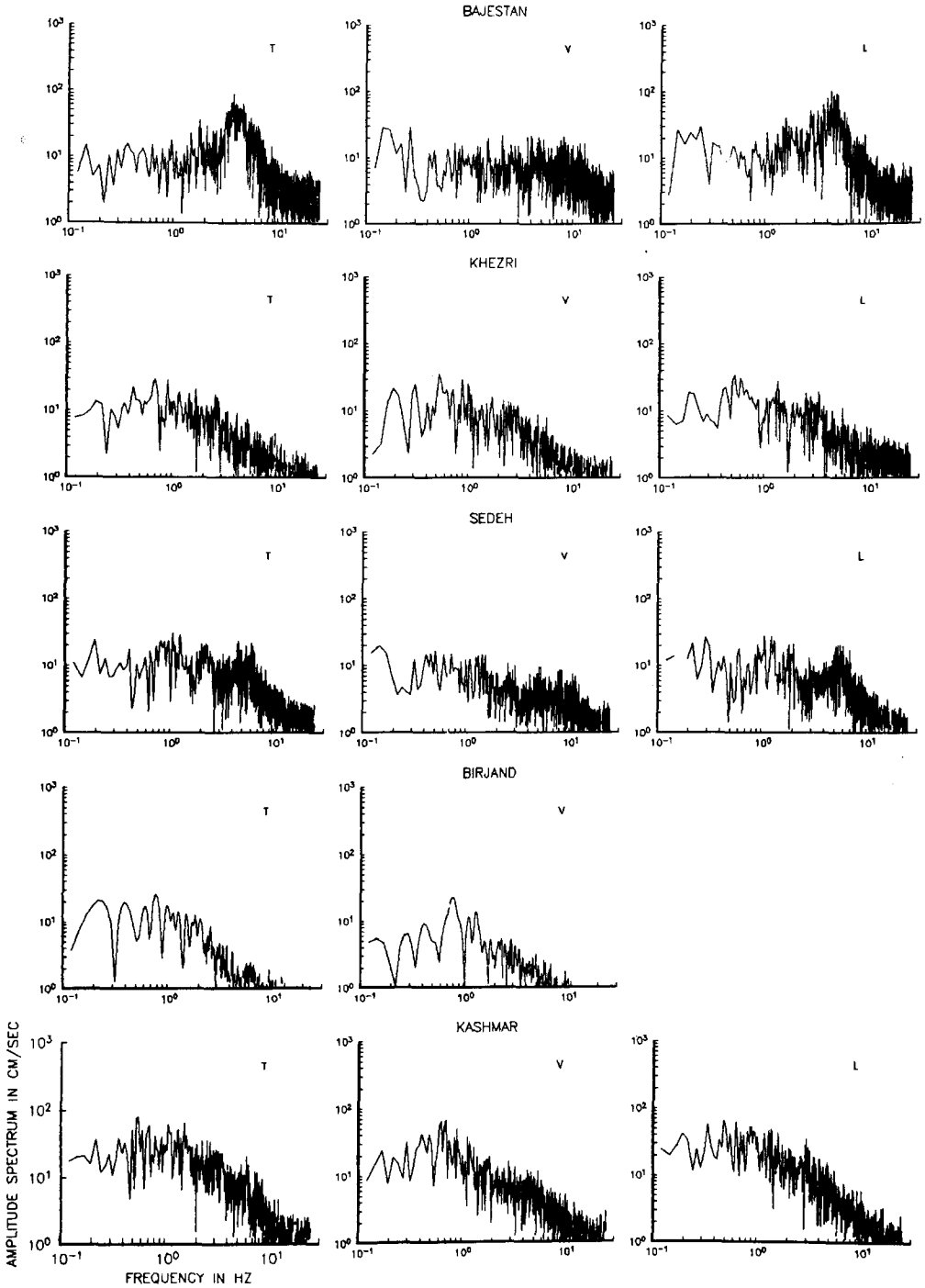


FIG. 10. Continued.

As described by Vassiliou and Kanamori (1982), there are two procedures available to estimate the radiated energy from seismograms. The first is invert for a source-time function and then determine the energy from that time function. The second is to directly integrate the observed waveform at one (or more) station and to infer

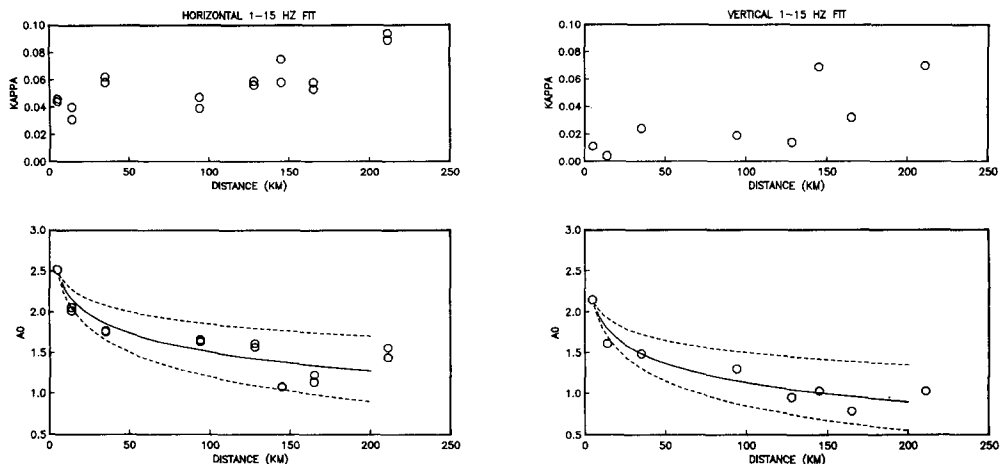


FIG. 11. Decay parameter, κ , and overall level, A_0 , from the Tabas spectra as a function of distance. Results for the horizontal components are shown on the *left*, and the vertical components are on the *right*.

energy based on the energy flux expected at the station, as determined by the geometry. Finding a model for the Tabas source-time function is beyond the scope of this study. Two variations on the second procedure are attempted here to estimate the energy radiated by the Tabas earthquake, one that is not significantly different from techniques that have been used in the past to find energy from strong motion records and a second which is somewhat innovative. Both approaches suffer from some limitations, which we will also discuss.

We begin by defining the integrals

$$I_t(t) = 0 \int_0^\infty v^2(t) dt \tag{2}$$

$$I_f(f) = 2 \int_0^\infty \tilde{v}^2(f) df \tag{3}$$

where $\tilde{v}(f)$ is the Fourier transform of the velocity, $v(t)$. We note that $I_t(\infty) = I_f(\infty)$. The integrals are shown in Figure 12 for the Tabas station and in Figure 13 for the Dayhook station. As was observed by Vassiliou and Kanamori (1982), by far most of the radiated energy is in waves with frequencies less than 1 to 2 Hz. This result is confirmed at the other stations also.

For a station near a finite fault, the relationship between integrated velocity and total radiated energy includes a geometrical term which depends on fault geometry, distance, radiation pattern, and focusing due to rupture propagation. Consider a surface, Σ , with area S_a which surrounds the fault. Then, provided all of the energy is flowing outward from the fault (no backscattering), the radiated energy could be obtained from a sufficiently dense sampling of $I_t(\infty)$ over Σ . With less data, one can assume that a single station is representative of every point on Σ . For this to work, Σ must be selected such that the energy flowing through it is expected to be as uniform as possible. The energy thus estimated from a single observation point may

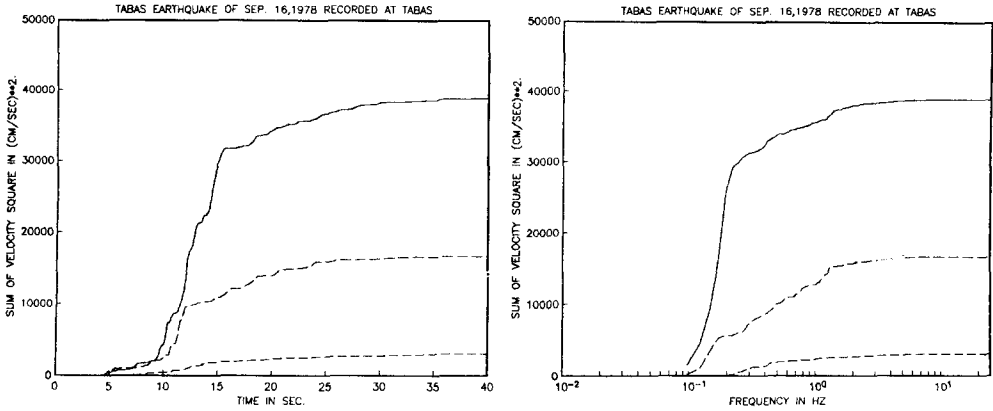


FIG. 12. Integrals of squared velocity from the Tabas accelerogram (left) and the corresponding integrals of the squared velocity spectrum (right).

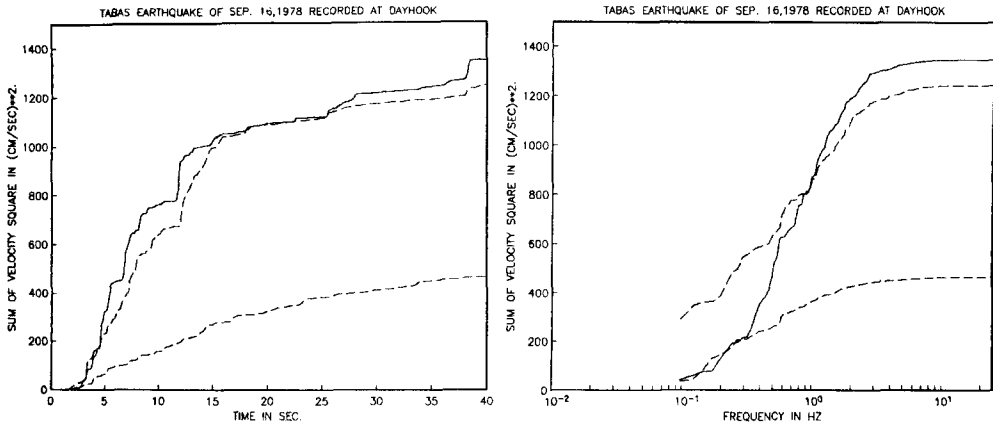


FIG. 13. Integrals of the squared velocity from the Dayhook accelerogram (left) and the corresponding integrals of the squared velocity spectrum (right).

be approximately written as

$$E = \frac{1}{4} \rho \beta S_a I_t(\infty). \tag{4}$$

In equation (4), we have assumed that all the waves cross the surface with velocity β . The density of the material is ρ . The quantity $\rho \beta I_t(\infty)$ is the energy flux, from Bullen (1963). The factor of $\frac{1}{4}$ comes from an assumption that observed velocities have been doubled by the surface of the earth. According to Bolt (1986), errors introduced by the assumptions that all waves travel with speed β and that free surface amplification is a factor of 2 are under 20 per cent in each case.

For large distances, R , compared to the fault dimension, the area S_a is the surface area of a sphere which surrounds the fault (Båth, 1966, p. 124),

$$S_a = 4\pi R^2. \tag{5}$$

Bolt (1986), after Bullen (1963) and Bullen and Bolt (1985), uses $S_a = 2\pi R^2$, based on the assumption that spherical spreading is confined to the lower side of the

focus. Trifunac (1972) and Anderson *et al.* (1986) approached the geometrical problem for strong motion stations directly above the fault by assuming the stations sampled the wave field from a uniformly radiating rupture of area A , and that the finite size of the fault had a negligible effect on the wave field. Under this approach,

$$S_a = 2A. \quad (6)$$

The approximations neglect the effects of the radiation pattern and focusing (e.g., Boatwright, 1980). For the Tabas geometry, both of these alternatives failed to capture the essential geometrical information because of the intermediate distance ranges of most of the stations.

For this situation, Sarma (1971) obtained a parameter, equivalent to S_a , based on uniform radiation of energy every place along the length of a rectangular fault. Schnabel and Seed (1973) defined a surface which goes through the station and surrounds the fault, and which consists of two planes offset from the sides of the fault, half-cylinders around the edges, and quarter spheres around the corners, all at a common distance from the nearest point of the fault. They took S_a as the surface area of that surface. We used the following scheme, which we will refer to as an "ellipsoidal normalization," which differs only slightly from Schnabel and Seed. We define the ellipsoid family

$$\left(\frac{x}{a+s}\right)^2 + \left(\frac{y}{b+s}\right)^2 + \left(\frac{z}{s}\right)^2 = 1 \quad (7)$$

where the fault lies in the $x - y$ plane and is approximated by an ellipse with axes a and b . This family of curves is asymptotic to a close bound for the elliptical approximation of the fault as s approaches zero and asymptotic to a sphere of radius s as s approaches infinity. Therefore, it provides a smooth transition between the two cases given by equations (5) and (6). The parameter s is determined to find the member of this family which goes through a station, and the surface area of that ellipsoid is taken as S_a . We found s and S_a numerically. Table 5 lists $I_t(\infty)$ for eight stations, the parameters s , the estimated surface areas S_a , and the energy estimates obtained by this technique. The geometric average of all eight stations is 2.6×10^{23} ergs. (We used the geometric mean rather than the arithmetic mean because it is not dominated by one or two outliers and because residuals on regressions, which are also affected by site effects, show a lognormal distribution.)

Using equations (4) and (5), we estimated the energies of the four subevents which appear on the Dayhook accelerogram. The result is that each of the four has about the same radiated energy, about 0.14×10^{23} ergs, which corresponds to $M_s \approx 7$.

For very close distances, the above technique would overestimate the total energy because of near-field terms (Anderson *et al.*, 1986). Also, radiation pattern and focusing have not been considered. We therefore tried an alternative, which we refer to as a "Haskell normalization," to estimate the energy. We calculated the synthetic velocity in an infinite, homogeneous medium from a propagating ramp dislocation model (Haskell, 1964, 1969; Boatwright and Boore, 1977) that seemed reasonable as a first approximation to the Tabas score. A model with Green's functions appropriate to the Tabas area would be better, but is beyond the scope of this paper. The total radiated energy from the propagating ramp is given by Haskell

TABLE 5
ENERGY CALCULATIONS FOR THE TABAS EARTHQUAKE

Station	$I_t(\infty)$ (cm^2/sec)	s^* (km)	S_a^* (km^2)	E_t^\dagger ($\times 10^{23}$ ergs)	$I_h(\infty)^\ddagger$	E_h^\S ($\times 10^{23}$ ergs)
Tabas	58,000	5	7,400	9.6	160.0	3.2
Dayhook	3,054	14	14,400	0.98	70.1	0.38
Boshrooyeh	1,995	35	32,900	1.5	40.5	0.44
Ferdows	474	94	165,000	1.7	2.31	1.8
Khezri	186	145	343,000	1.4	1.37	1.2
Bajestan	342	128	277,000	2.1	1.55	2.0
Sedeh	205	165	429,000	2.0	0.146	12.0
Kashmar	814	211	668,000	12.0	0.510	14.0

* s and S_a are distance parameters of the surface area for the family of ellipsoids defined in equation (7).

† Energy based on ellipsoidal normalization [$\beta = 3.3$ km/sec, $\rho = 2.75$ gm/cm³ in equation (4)].

‡ The parameters of the Haskell model which were employed to generate the synthetic velocities are fault length = 80 km, fault width = 30 km, rupture velocity = 2.7 km/sec, rise time = 10 sec, offset = 225 cm (pure thrust), fault strike = 324°, fault dip = 30°, south corner of fault is at the surface, at coordinates 33.16°N, 57.35°W. The radiated energy from this model is 3.54×10^{21} ergs.

§ Energy based on Haskell normalization.

(1964). The velocity synthetic seismogram for each station was integrated, as in equation (4), to obtain $I_h(\infty)$. Finally, the energy was estimated by multiplying the energy from the propagating ramp by the ratio $I_t(\infty)/4I_h(\infty)$ where the factor of $\frac{1}{4}$ comes from the assumption that observed velocity has been doubled by the free surface. The ratio is on the order of 100 and is consistent with the result reported by Haskell (1964) that the smooth propagating ramp radiates too little energy. Jack Boatwright (personal communication) has pointed out that the discrepancy which Haskell found between the radiated energy of a smooth rupture approximation to the 1952 Kamchatka earthquake and the energy inferred from the magnitude might not withstand scrutiny. Within the uncertainties of the parameters to describe the earthquake, a Haskell model can radiate significantly more energy than the particular parameterization considered by Haskell (1964). On the other hand, the magnitude scale used by Haskell was probably saturated. Thus, there is a basis to doubt both sides of Haskell's comparison. In any case, there is little debate that the Haskell (1964) model of a smooth propagating ramp is too smooth to be considered realistic as an earthquake source. Thus, we are not surprised by the large ratio of observed to calculated velocity-squared integrals.

The energy estimates are shown, as a function of the ellipsoidal parameter s , in Figure 14. The greatest differences between the two normalizations occur for the station Sedeh, which is six times larger under the Haskell normalization, and Boshrooyeh, which is three to four times smaller. At all of the other stations, the differences between the two approaches are less than a factor of 2. The variance is somewhat greater under the Haskell normalization. Due to the limitations of the Haskell model (e.g., Madariaga, 1978), we are reluctant to give the Haskell normalization more credence than the ellipsoidal normalization.

It was seen earlier that, as expected near a finite source, the peaks of the filtered accelerograms fall off less rapidly than body waves from a point source. Both normalizations imply an effective distance dependence from the nearest faulting which is less rapid than $1/R$, even though both are asymptotic to $1/R$ at large distances. The normalizations both also give a distance dependence which resembles the distance dependence proposed by Gusev (1983).

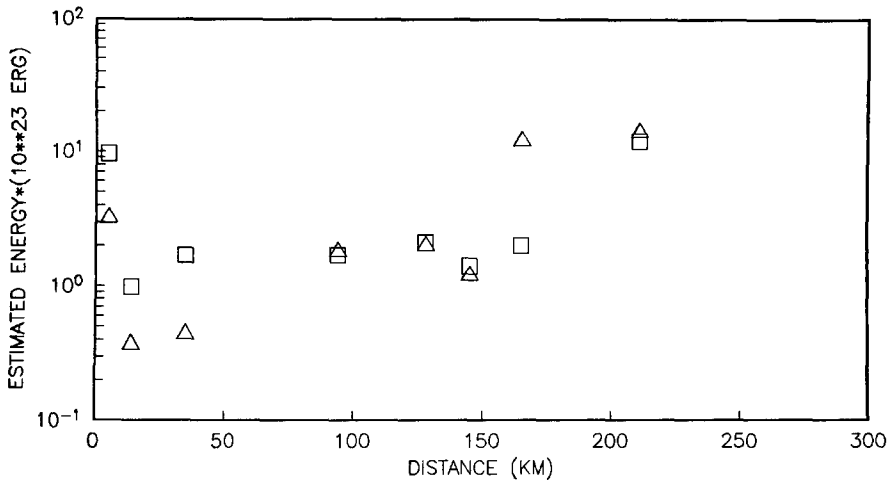


FIG. 14. Energy estimates for the Tabas earthquake by two different methods (as described in the text) shown as a function of distance of the station to the fault. Results obtained using the ellipsoidal normalization are represented by squares, and results obtained using the Haskell normalization are represented by triangles.

Even though the distance dependence, which is built into these normalizations, is already less rapid than $1/R$ body-wave spreading from a point source, these energy estimates, like previous near-field estimates, have neglected the difference between geometrical spreading in an infinite medium and in the earth, where energy is trapped near the surface. In Figure 14, this effect would show an increase in the estimated energy with greater distance as the result of increasing contributions of surface waves. Curiously, at large distances, Kashmar (the point beyond 200 km) is the only station that might show this effect. The high-energy estimate for Sedeh (165 km) under the Haskell normalization is because the station is nodal for the particular faulting model which we employed (see Table 5).

Another neglected effect is surface amplification, for which there are two aspects. The first is the usual amplification expected from the decrease of rigidity as the seismic waves approach the surface (Haskell, 1960). We expect that this effect is least important in Dayhook because we believe that the sediments there are only a thin veneer. This is consistent with Dayhook yielding the smallest estimates for the radiated energy. The second, which is probably acting at the Tabas station to increase the energy estimate there dramatically compared to other close-in stations, is additional amplification caused by passage of the rupture at a speed which is smaller than the shear velocity in the basement but greater than the shear velocity in the overlying sediments. Bouchon (1979) and Mendez and Luco (1987) have found this effect to enhance amplitudes by nearly a factor of 10.

We can compare our energy estimates with estimates by other procedures. A static estimate for the energy, from the moment (Vassiliou and Kanamori, 1982), is 7.5×10^{22} ergs, a factor of 3 less than our estimates from the seismograms. Our energy estimates (2.6 and 2.1×10^{23} erg) both exceed the Gutenberg and Richter (1954) energy formula with $M_S = 7.4$, which gives $E = 7.9 \times 10^{22}$ ergs. Most of the earthquakes studied by Vassiliou and Kanamori (1982) radiated less energy than the Gutenberg and Richter curve predicts, perhaps indicating that the Tabas event was more energetic than average. However, from the preferred P -wave source model in Niazi and Kanamori (1981) and using the Vassiliou and Kanamori equation for

the energy, one teleseismic estimate for the radiated energy is 9.1×10^{21} ergs. The Vassiliou and Kanamori formula is based on a smooth, Haskell (1964) propagating ramp. Boatwright and Choy (1987) applied the procedure in Boatwright and Choy (1986) to obtain estimates of radiated energy from teleseisms ranging from 4.3 to 8×10^{21} ergs. These estimates are one to two orders of magnitude smaller than what we have obtained from the strong motion records. Thus, it appears that it is premature to conclude that the Tabas earthquake has a higher than average energy because there is a major discrepancy between teleseismic and near-field estimates of seismic energy for this earthquake. The most optimistic way to reduce the discrepancy from the strong motion side is to consider the Dayhook station to be most reliable, since supposedly the sediment amplification effects are smallest there and directivity related to surface waves would be decreasing amplitudes there. Even for this station, however, taking maximum advantage of uncertainties in the quantities in equation (4), energies are significantly greater than the teleseismic estimates.

Stress drops. Empirical and theoretical relations involving seismic source parameters are employed here in an attempt to estimate the various stress change parameters. We noted previously (Table 1) that Berberian (1979) estimated that the static stress drop during the earthquake was 25 bars.

For an infinite fault with infinite rupture velocity, Brune (1970, 1971) gives a relation

$$\dot{U}_0 = \sigma \frac{\beta}{\mu} \quad (8)$$

where U_0 is the particle velocity close to the fault, β is the shear velocity, and $\sigma = \sigma_0 - \sigma_f$ (σ_0 is initial stress and σ_f is frictional stress) is the effective dynamic stress. For a more distant station, geometrical spreading becomes important, and for the Brune model, McGarr *et al.* (1981) used

$$\dot{U}_0 = 0.57 \left(\frac{r}{R} \right) \left(\frac{\sigma}{\mu} \right) \beta \quad (9)$$

where r is the radius of the source or asperity, and R is the source to station distance. For finite rupture velocity, it can be shown that (Kanamori, 1972)

$$\dot{U}_0 = C \frac{\sigma}{\mu} \beta \quad (10)$$

where $C = (1 + \beta/\nu)$ in which ν is rupture velocity. In applying these equations, we assume that observed velocities have been doubled because of the free surface.

We apply these relations to the horizontal components recorded at Tabas and Dayhook sites with the effective source distances of 3 and 14 km, respectively, to infer the effective dynamic stress during this earthquake. In subsequent calculations, we shall use the shear velocity $\beta = 3.3$ km/sec, shear modulus $\mu = 3.0 \times 10^{11}$ dyne/cm², and rupture velocity $\nu = 2.7$ km/sec.

Equations (8) to (10) are used to estimate $\sigma_0 - \sigma_f$. The combined value of horizontal $\dot{U}_{\max} \approx 130$ cm/sec recorded at the Tabas site (see Figure 5) gives, using

equation (8)

$$\sigma_0 - \sigma_f \approx 60 \text{ bars.}$$

If we assume a subsource of radius of 8 km, corresponding to half the distance between subevents 1 and 2, the value of $\dot{U}_{\max} \approx 30$ cm/sec recorded at the Dayhook site gives, using equation (9)

$$\sigma_0 - \sigma_f \approx 40 \text{ bars.}$$

Based on our estimate for the seismic energy, the "Orowan stress drop" (Vassiliou and Kanamori, 1982), which is equal to twice the apparent stress (Aki, 1966; Savage and Wood, 1971; Wyss and Molnar, 1972), is 90 bars, which is somewhat larger than the stress drops previously given and somewhat larger than the worldwide average of 20 to 60 bars.

Site effects. There are several indications that site effects are important at some stations. Unfortunately, detailed profiles of the structure below the sites have not been determined. Among the most critical close-in stations, the Dayhook site is probably on thin sediments, located on the flank of limestone hills. This may have caused the motion to be less amplified than Tabas and perhaps other sites. Tabas is located on a thick alluvial deposit which may have caused some amplification at that site, but we have no reason, other than the seismograms, to believe it is greater here than at the other stations. The spectra from Bajestan show a peak at about 4 Hz, which has not noticeably affected the energy estimates, but perhaps the peak acceleration and some of the filtered peaks have been increased. By every criteria, the accelerogram at Kashmar appears to have been amplified by site effects. The peak values of acceleration, velocity, and filtered acceleration are high, the spectra of the two components are higher than four closer stations, and the energy estimated from the station is a factor of 6 larger than the average.

CONCLUSIONS

In this paper, we interpreted the strong motion records of the 1978 Tabas earthquake to investigate the complexity of the source of this earthquake in some detail, construct attenuation curves for values of acceleration, velocity, and band-passed accelerograms, and estimate some of the source parameters such as seismic energy release and stress drops. The results may be summarized as follows.

1. The relatively compact arrivals of strong signals on Tabas records and rather widely distributed arrivals of the strong signals on Dayhook records together with other evidence (e.g., location of the epicenter and aftershock distribution) strongly suggest that the rupture was initiated near the site of Dayhook and propagated toward Tabas. The inferred epicenter from the strong motion records is about 20 km southwest of Dayhook and several kilometers south of the reported epicenters. It was shown that the earthquake was a multiple shock consisting of at least four distinct bursts of energy distributed along the fault length. Based on the relative arrival times of these subevents at the near stations, the velocity of rupture propagation was estimated as 2.7 ± 0.2 km/sec. This agrees with the 2.5 km/sec value obtained by Niazi (1984).
2. The peak values of acceleration and velocity of the Tabas earthquake are employed to infer attenuation curves for this earthquake (Table 4). Comparison of these peak values with the prediction curves recently proposed for the

Western United States show systematic differences which depend on distance, on whether we consider velocity or acceleration, and on the definition of distance employed in the regression. Peak ground acceleration and peak ground velocity values of two other large intraplate thrust earthquakes, Kern County, California (1952) and Gazli, USSR (1976), which also produced close-in strong motion records, are consistent with the trend of the Tabas peak values. We conclude that the differences might be systematic for this size and type of earthquake.

3. We estimated the total radiated energy for two procedures, an "ellipsoidal normalization" for which the geometric average of energy of eight stations is 2.6×10^{23} ergs, and a "Haskell normalization," which gives a geometric average of 2.1×10^{23} ergs.

The conceptual advantage of the Haskell normalization is that it accounts for radiation pattern, focusing, and near-field contributions to the velocity, while the ellipsoidal normalization does not compensate for these effects at all. The Haskell normalization may overcompensate, however, because of the unrealistic aspects of the kinematical faulting description which suppresses radiation of high frequencies. The advantage of the ellipsoidal normalization is that it provides an empirical scheme to allow a smooth transition from the far-field, where it is reasonable to approximate the energy as transmitted across the surface of a sphere, to close points where it is more reasonable to approximate the energy as being radiated outward from a plane. Both estimates give energy greater than the Gutenberg and Richter (1954) energy formula with $M_S = 7.4$, which gives $E = 7.9 \times 10^{22}$ ergs, and substantially larger than estimated energy based on teleseismic analysis of this earthquake.

We estimated the energies of the four subevents appearing on the Dayhook accelerogram. The result is that each of the four has about the same radiated energy (about 0.14×10^{23} ergs) which corresponds to $M_S \approx 7$.

The "Orowan stress drop" estimated from the radiated energy is 90 bars, larger than the worldwide average of 20 to 60 bars.

Employing the combined value of horizontal peak velocity recorded at the Tabas and Dayhook sites (nearest site to the source), we estimated the effective dynamic stress as 50 to 60 bars.

4. The site effects seem important at some stations. The spectra from Bajestan show a peak of about 4 Hz, which may have increased the peak acceleration and some of the filtered peaks. From the estimated energy at Tabas and Dayhook, they show some amplification and deamplification, respectively. By every criteria, the accelerogram at Kashmar appears to have been amplified by site effects, since the peak values of acceleration, velocity, and filtered acceleration are high, the spectra of the two components are higher than four closer stations, and the energy estimated for the station is a factor of 6 larger than the average.

ACKNOWLEDGMENTS

J. Shoja-Taheri acknowledges the financial support of Mashad University and thanks J. Brune and the Institute of Geophysics and Planetary Physics for inviting him to spend his sabbatical leave there. A. A. Moïfar responded to our questions regarding the site conditions of the accelerograph stations. We thank J. Brune, E. Luco, and A. Olson for helpful discussions during the course of this research. J. E. Luco had suggested the use of the parameter s [equation (7)] as a distance measure for peak value regressions prior to our application. J. Boatwright, D. M. Boore, J. E. Luco, and M. Niazi critically

reviewed the manuscript. The research was supported by National Science Foundation Grants CEE 83 19620 and ECE 85 13489.

REFERENCES

- Aki, K. (1966). Generation and propagation of *G* waves from the Niigata earthquake of June 16, 1964, *Bull. Earthquake Res. Inst., Tokyo Univ.* **44**, 23–88.
- Anderson, J. G. (1986). Implication of attenuation for studies of the earthquake source, in *Earthquake Source Mechanics*, S. Das, J. Boatwright, and C. H. Scholz, Editors, Geophysics Monograph 37, Maurice Ewing Series 6, American Geophysical Union, Washington, D.C., 311–318.
- Anderson, J. G. and S. E. Hough (1984). A model for the shape of the Fourier amplitude of spectrum of acceleration at high frequencies, *Bull. Seism. Soc. Am.* **73**, 1969–1994.
- Anderson, J. G., P. Bodin, J. Brune, J. Prince, S. K. Singh, R. Quaas, and M. Onate (1986). Strong ground motion from the Michoacan, Mexico earthquake, *Science* **233**, 1043–1049.
- Báth, M. (1966). Earthquake energy and magnitude, in *Physics and Chemistry of the Earth*, vol. 7, L. H. Ahrens, F. Press, S. K. Runcom, and H. C. Urey, Editors, Pergamon Press, Oxford, England, 117–165.
- Berberian, M. (1979). Earthquake faulting and bedding thrust associated with the Tabas-e-Golshan (Iran) earthquake of September 16, 1978, *Bull. Seism. Soc. Am.* **69**, 1861–1887.
- Berberian, M. (1982). Aftershock tectonics of the 1978 Tabas-e-Golshan (Iran) earthquake sequence: a documented active thin and thick skinned tectonic case, *Geophys. J. Astr. Soc.* **68**, 499–530.
- Berberian, M., I. Asudeh, R. G. Bilham, C. H. Scholz, and C. Soufleris (1979). Mechanism of the main shock and the aftershock study of the Tabas-e-Golshan (Iran) earthquake of September 16, 1978: a preliminary report, *Bull. Seism. Soc. Am.* **69**, 1851–1859.
- Boatwright, J. (1980). A spectral theory for circular seismic sources; simple estimates of source dimension, dynamic stress drop, and radiated seismic energy, *Bull. Seism. Soc. Am.* **70**, 1–27.
- Boatwright, J. and D. M. Boore (1977). A simplification in the calculation of motions near a propagating dislocation, *Bull. Seism. Soc. Am.* **65**, 133–138.
- Boatwright, J. and G. L. Choy (1986). Teleseismic estimates of the energy radiated by shallow earthquakes, *J. Geophys. Res.* **91**, 2095–2112.
- Boatwright, J. and G. L. Choy (1987). Acceleration source spectra for large earthquakes in northeastern North America, Presented at the EPRI Workshop on Earthquake Ground Motion Estimation in eastern North America, March 1987, Palo Alto, California.
- Bolt, B. A. (1986). Seismic energy release over a broad frequency band, *Pageoph* **124**, 919–930.
- Bolt, B. A. and N. A. Abrahamson (1982). New attenuations of strong ground motion, *Bull. Seism. Soc. Am.* **72**, 2307–2322.
- Boore, D. M. (1980). On the attenuation of peak velocity, *Proceedings 7th World Conference on Earthquake Engineering*, Istanbul, Turkey.
- Bouchon, M. (1979). Predictability of ground displacement and velocity near an earthquake fault: an example, the Parkfield earthquake of 1966, *J. Geophys. Res.* **84**, 6149–6156.
- Brillinger, D. R. and H. K. Priesler (1984). An exploratory analysis of the Joyner-Boore attenuation data, *Bull. Seism. Soc. Am.* **72**, 1441–1450.
- Brune, J. (1970). Tectonic stress and the spectra of seismic shear waves from earthquakes, *J. Geophys. Res.* **75**, 4997–5009.
- Brune, J. (1971). Correction, *J. Geophys. Res.* **76**, 5002.
- Bullen, K. E. (1963). *An Introduction to the Theory of Seismology*, 3rd ed., Cambridge University Press, Cambridge, England, 381 pp.
- Bullen, K. E. and B. A. Bolt (1985). *An Introduction to the Theory of Seismology*, 4th ed., Cambridge University Press, Cambridge, England, 499 pp.
- Bulletin of the Seismographic Network of Mashad University (BSNMU) (1984). Epicenter listing for July 1–December 31, 1978.
- Campbell, K. W. (1981). Near-source attenuation of peak horizontal acceleration, *Bull. Seism. Soc. Am.* **71**, 2039–2070.
- Chandra, V., J. G. McWhorten, and A. A. Nowroozi (1979). Attenuation of intensities in Iran, *Bull. Seism. Soc. Am.* **69**, 237–250.
- Dunbar, S., D. M. Boore, and W. Thatcher (1980). Pre-, co-, and post-seismic strain changes associated with the 1952 $M_L = 7.2$ Kern County California earthquake, *Bull. Seism. Soc. Am.* **70**, 1501–1523.
- Geller, R. J. (1976). Scaling relations for earthquake source parameters and magnitudes, *Bull. Seism. Soc. Am.* **66**, 1501–1523.

- Gusev, A. A. (1983). Descriptive statistical model of earthquake source radiation and its application to an estimation of short-period strong motion, *Geophys. J. R. Astr. Soc.* **74**, 787-808.
- Gutenberg, B. and C. F. Richter (1952). *Seismicity of the Earth and Associated Phenomena*, Princeton University Press, Princeton, New Jersey.
- Hadley, D. M. and G. R. Mellman (1982). Summaries of technical reports XIV, National Earthquake Hazard Reduction Program, *U.S. Geol. Surv., Open-File Rept. 82-840*, 175-178.
- Hadley, D. M., H. G. Hawkins, and K. L. Benushka (1983). Strong ground motion record of the 16 September 1978 Tabas, Iran, earthquake, *Bull. Seism. Soc. Am.* **73**, 315-320.
- Hartzell, S. H. (1980). Faulting process of the May 17, 1976 Gazli, USSR earthquake, *Bull. Seism. Soc. Am.* **70**, 1715-1736.
- Haskell, N. A. (1960). Crustal reflection of plane SH waves, *J. Geophys. Res.* **65**, 4147-4150.
- Haskell, N. A. (1964). Total energy and energy spectral density of elastic wave propagation from propagating faults, *Bull. Seism. Soc. Am.* **54**, 1811-1841.
- Haskell, N. A. (1969). Elastic displacement in the near-field of a propagating fault, *Bull. Seism. Soc. Am.* **59**, 865-908.
- Hough, S. E. and J. G. Anderson (1988). High-frequency spectra observed at Anza, California: implications for Q structure, *Bull. Seism. Soc. Am.* **78** (in press).
- Hough, S. E., J. G. Anderson, J. N. Brune, F. L. Vernon, III, J. Berger, J. Fletcher, L. Haar, T. Hanks, and L. Baker (1988). Attenuation near Anza, California, *Bull. Seism. Soc. Am.* **78** (in press).
- Howell, B. F., Jr. and T. R. Schultz (1975). Attenuation of Modified Mercalli intensity with distance from the epicenter, *Bull. Seism. Soc. Am.* **65**, 651-665.
- Jennings, P. C. and H. Kanamori (1983). Effect of distance on local magnitudes found from strong motion records, *Bull. Seism. Soc. Am.* **73**, 265-280.
- Joyner, W. B. and D. M. Boore (1981). Peak horizontal acceleration and velocity from strong-motion records including records from the 1979 Imperial Valley, California earthquake, *Bull. Seism. Soc. Am.* **71**, 2011-2038.
- Joyner, W. B. and D. M. Boore (1982). Prediction of earthquake response spectra, *U.S. Geol. Surv., Open-File Rept. 82-977*.
- Joyner, W. B., D. M. Boore, and R. L. Porcella (1981). Peak horizontal acceleration and velocity from strong-motion records (abstract), *Earthquake Notes* **52**, 80-81.
- Kanamori, H. (1972). Determination of effective tectonic stress associated with earthquake faulting. The Totteri earthquake of 1943, *Phys. Earth Planet. Interiors* **5**, 426-434.
- Kanamori, H. and P. C. Jennings (1978). Determination of local magnitude, M_L , from strong-motion accelerograms, *Bull. Seism. Soc. Am.* **68**, 471-485.
- Luco, J. E. (1982). A note on near-source estimates of local magnitude, *Bull. Seism. Soc. Am.* **72**, 941-958.
- Luco, J. E. and J. G. Anderson (1983). Steady-state response of an elastic half-space to a moving dislocation of finite width, *Bull. Seism. Soc. Am.* **73**, 1-22.
- Luco, J. E. and J. G. Anderson (1985). Near source ground motion from kinematic fault models, in *Proceedings: Strong Ground Motion Simulation and Earthquake Engineering Applications*, R. Scholl and J. King, Editors, Earthquake Engineering Research Institute/Electric Power Research Institute, Palo Alto, California, 18-1-18-20.
- Madariaga, R. (1978). The dynamic field of Haskell's rectangular dislocation fault model, *Bull. Seism. Soc. Am.* **68**, 869-887.
- McGarr, A., R. W. E. Green, and S. M. Spottiswoode (1981). Strong ground motion of mine tremors: some implications for near-source ground motion parameters, *Bull. Seism. Soc. Am.* **71**, 295-319.
- Mendez, A. and J. E. Luco (1987). Simulation of a near-field earthquake ground motion by a steady-state dislocation model in a layered half-space (abstract), SSA Meeting, March 1987, Santa Barbara, California.
- Mohajer-Ashjai, A. and A. A. Nowroozi (1979). The Tabas earthquake of September 16, 1978 in east-central Iran: a preliminary field report, *Geophys. Res. Letters* **6**, 689-692.
- Moinfar, A. A. and H. Adibnazari (1982). The Tabas earthquake of 16th September 1978, Technical Report #47, Building and Housing Research Center, Ministry of Housing and Urban Development, Islamic Republic of Iran.
- Murphy, L. M. and W. K. Cloud (1952). United States Earthquakes 1952, U.S. Department of Commerce Coast and Geodetic Survey, Series No. 773, Washington, D.C., 112 pp.
- Niazi, M. (1984). Estimation of rupture velocity and near field Q from the Tabas accelerogram of the September 16, 1978, Iran earthquake, *Proceedings of the 8th World Conference on Earthquake Engineering*, vol. II, San Francisco, California, 377-383.
- Niazi, M. (1986). Accelerograms of the 1978 Tabas, Iran, earthquake, *Earthquake Spectra* **2**, 635-651.

- Niazi, M. and H. Kanamori (1981). Source parameters of 1978 Tabas and 1979 Qainat, Iran, earthquakes from long-period surface waves, *Bull. Seism. Soc. Am.* **71**, 1201-1213.
- Niazi, M. and J. Shoja-Taheri (1985). Source geometry and mechanism of 1978 Tabas, Iran earthquake from well-located earthquakes, *Tectonophysics* **115**, 61-68.
- National Iran Oil Company (NIOC) (1977). Geological map of Iran, 1:1,000,000, sheets 2, 3, and 5.
- Nuttli, O. W. (1980). The excitation and attenuation of seismic crustal phases in Iran, *Bull. Seism. Soc. Am.* **70**, 469-485.
- Richter, C. F. (1935). An instrumental earthquake scale, *Bull. Seism. Soc. Am.* **25**, 1-32.
- Richter, C. F. (1958). *Elementary Seismology*, W. H. Freeman and Co., San Francisco, California, 768 pp.
- Sarma, S. K. (1971). Energy flux of strong earthquakes, *Tectonophysics* **11**, 159-173.
- Savage, J. C. and M. D. Wood (1971). The relation between apparent stress and stress drop, *Bull. Seism. Soc. Am.* **61**, 1381-1388.
- Schnabel, P. B. and H. B. Seed (1973). Accelerations in rock for earthquakes in the western United States, *Bull. Seism. Soc. Am.* **63**, 501-516.
- Shoja-Taheri, J. (1977). Seismological studies of strong motion records, UCB/EERC-77/04, University of California at Berkeley, California.
- Shoja-Taheri, J. (1984). Accelerograms of the 1978 Tabas (Iran) earthquake: the generalized records and correlations between the strong motion parameters in different frequency bands, Presented at the Regional Assembly of IASPEI, Hyderabad, India.
- Shoja-Taheri, J. and B. A. Bolt (1977). A generalized strong motion accelerogram based on spectral maximization from two horizontal components, *Bull. Seism. Soc. Am.* **67**, 863-876.
- Trifunac, M. D. (1972). Stress estimates for the San Fernando, California earthquake of February 9, 1971: main event and thirteen aftershocks, *Bull. Seism. Soc. Am.* **62**, 724-750.
- Trifunac, M. D. and V. W. Lee (1978). Uniformly processed strong earthquake ground accelerations in the Western United States of America for the period from 1933 to 1971: corrected acceleration velocity and displacement curves, Report No. CE-7801, Department of Civil Engineering, University of Southern California, Los Angeles, California.
- Vassiliou, M. S. and H. Kanamori (1982). The energy release in earthquakes, *Bull. Seism. Soc. Am.* **72**, 371-387.
- Wyss, M. and P. Molnar (1972). Source parameters of intermediate and deep focus earthquakes in the Tonga Arc, *Phys. Earth Planet. Interiors* **6**, 279-292.

SCHOOL OF SCIENCES
MASHAD UNIVERSITY
MASHAD, IRAN (J.S.T.)

INSTITUTE OF GEOPHYSICS AND
PLANETARY PHYSICS
SCRIPPS INSTITUTION OF OCEANOGRAPHY
UNIVERSITY OF CALIFORNIA
AT SAN DIEGO
LA JOLLA, CALIFORNIA 92093 (J.G.A.)

Manuscript received 10 August 1986